Czech Technical University in Prague
Faculty of Nuclear Sciences and Physical Engineering

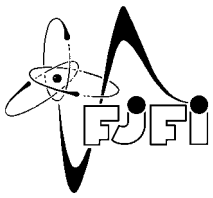

Semi-inclusive p_T spectra of jets in light systems at the LHC energies

Semi-inkluzivní p_T spektra jetů v lehkých systémech na LHC

Bachelor's Degree Project

Author: **Peter Príbeli**

Supervisor: **RNDr. Filip Křížek, Ph.D.**

Academic year: 2015/2016

- Zadání práce -

- Zadání práce (zadní strana) -

Acknowledgment:
I would like to thank Filip Křížek for his expert guidance and express my gratitude to my family for their loving support.

Author's declaration:
I declare that this Bachelor's Degree Project is entirely my own work and I have listed all the used sources in the bibliography.

Prague, July 7, 2016 Peter Príbeli

Název práce:

Semi-inkluzivní p_T spektra jetů v lehkých systémech na LHC

Autor: Peter Príbeli

Obor: Experimentální jaderná a částicová fyzika

Druh práce: Bakalářská práce

Vedoucí práce: RNDr. Filip Křížek Ph.D., Ústav jaderné fyziky AV ČR, v.v.i.

Abstrakt: Práce shrnuje základní myšlenky Kvantové Chromodynamiky (QCD) a popisu silné interakce. V této souvislosti se dále zabýváme popisem jetů, kolimovaných sprškek částic vznikajících při fragmentaci kvarků a gluonů. Podáváme popis používaných jetových algoritmů a jejich základních vlastností. Na základě pp, $\sqrt{s} = 7$ TeV případů simulovaných generátorem PYTHIA ověřujeme metody korekce měřených spekter nabitých jetů na detektorové efekty.

Klíčová slova: anti-k_t jet algoritmus, jet, QCD, SVD dekonvoluce, silná interakce, tvrdý proces

Title:

Semi-inclusive p_T spectra of jets in light systems at the LHC energies

Author: Peter Príbeli

Abstract: The thesis reviews the basic ideas of Quantum Chromodynamics (QCD) and the description of the Strong interaction. In this context, we further explore the concept of jets, collimated particle showers, that arises due to the fragmentation of quarks or gluons. We put forward a description of the used jet algorithms and their properties. We verify the methods of correcting the measured spectra of charged jets on detector effects based on pp data simulated by PYTHIA.

Key words: anti-k_t jet algorithm, hard process, jet, QCD, SVD unfolding, Strong interaction

Contents

List of Symbols

Physical Constants

α_s The strength of the strong interaction ≈ 1

$\hbar$ The reduced Planck's constant. $\hbar = \frac{h}{2\pi}$ $\approx 1.0546 \times 10^{-34}$ J s

c The speed of light in vacuum $299,792,458$ m/s

g_{QCD} The QCD coupling constant

Mathematical symbols

$:=$ A definition

$< \hat{\phi} >_{\psi}$ The expectation value of the operator $\hat{\phi}$ acting on ψ

$[A, B]$ The commutator of A and B

$[a, b]$ A closed interval

δ_{μ}^{ν} The Dirac delta function

$\hat{\mathcal{H}}$ An operator

$\mathbb{A}^T$ The transpose of a matrix $\mathbb{A}$

$\mathbb{A}^{-1}$ The inverse of a matrix $\mathbb{A}$

$\mathbb{C}$ The set of complex numbers

$\mathbb{C}^{n,m}$ The space of complex $n \times m$ matrices

$\mathbb{N}$ The set of natural numbers

$\mathbb{R}$ The set of real numbers

$\mathcal{O}$ The big $\mathcal{O}$ notation

$\text{diag}\,(x_1, x_2, ..., x_n)$ A diagonal matrix with the values $x_1, x_2, ..., x_n$ on its diagonal

$\text{rank}(\mathbb{A})$ The rank of the matrix $\mathbb{A}$

$\text{Tr}(\mathbb{A})$ The trace of the matrix $\mathbb{A}$

$\mathscr{H}$ A Hilbert space

$\overline{A}$ The complex conjugate of A

$\overline{M}$ The closure of a set M

$\psi^{\dagger}$ The Hermitian conjugate of ψ

$\not{X}$ The Feynman slash notation

$E[x]$ The expectation value of x

f^{abc} The structure constants

i The imaginary unit

$N(\mu, \sigma)$ The normal distribution with mean μ and standard deviation σ

Other Symbols

e.g. *(exempli gratia)* For example

etc *(et cetera)* And other things

Physical quantities

$\dot{q}$ The generalized velocity

η The pseudorapidity

$\mathcal{H}$ The Hamiltonian

$\mathcal{L}$ The Lagrangian

$\mathcal{S}$ The action

$\mathscr{L}$	The Lagrangian density
μ, ν	4-vector indices
ϕ	The azimuthal angle
ψ	The wavefunction
a, b, c	Colour indices
A^a_μ	The vector (gauge) potential
D_μ	The covariant derivative
$F_{\mu\nu}$	The electromagnetic field tensor
$g_{\mu\nu}$	The metric tensor
$G^a_{\mu\nu}$	The gluon field strength tensor
J^P	The total angular momentum
m	Mass
p	The generalized momentum
p_T	The transverse momentum
Q	The momentum transfer of a collision
q	The generalized position
T	The kinetic energy
t	Time
T_3	The third component of the isospin
U	The potential energy
Y	The hypercharge
y	The rapidity

Introduction

Quantum Chromodynamics (QCD), the theory describing the strong interactions of quarks and gluons, predicts a new state of matter—*Quark-Gluon Plasma (QGP)* [1]. QGP is a state where quarks and gluons are no longer confined to hadrons. In the limit of high temperature and energy densities, the dynamics of quarks and gluons in QGP should be driven by the asymptotic freedom limit of QCD [2]. According to lattice QCD calculations [3], the transition from a hadron gas to QGP occurs at temperatures above 160 MeV. These conditions are met for fractions of a second in heavy-ion collisions at particle accelerators such as the Relativistic Heavy Ion Collider (RHIC) or the Large Hadron Collider (LHC).

One possible option for the characterization of the properties of QGP is to use a self-generated probe from hard scattering of partons. Hard scattering occurs in the initial phase of the collision and produces partons (quarks/gluons) with high transverse momenta (p_T). These high-p_T partons fragment into high energy jets and travel through the hot and dense nuclear medium. On the way, the high energy jets interact with the QGP and lose energy via various processes. The so-called *jet quenching* phenomenon [4], [5], [6], [7], [8] is observed as a result. It is manifested by a suppressed production of high p_T jets when compared to the expectations based on binary collision scaled jet yield from proton-proton collisions. Since jet production is well understood in elementary processes, jet quenching can be used to gain information about the jet-medium interaction and the structure of QGP, as originally suggested by Bjorken [9].

The study of jet quenching in heavy ion collisions faces a problem of distinguishing quenched jets from a large underlying event background. One possible approach uses semi-inclusive spectra of charged jets recoiling from a high-p_T trigger hadron (simultaneous production of a hadron and a jet in back-to-back coincidence) [10]. Medium induced modifications of jet fragmentation are revealed and quantified by comparing per trigger normalized jet yields obtained in heavy ion collisions with the yield measured in lighter systems such as pp or p-Pb.

The goals of the thesis can be summarized as follows:

- To explore the basic description of hard processes that occur in nucleon-nucleon collisions at high centre-of-mass energies,
- To get familiar with the properties of the k_t and anti-k_t jet algorithms,
- To verify the procedures used to correct jet spectra on detector effects utilizing simulations of proton-proton collisions in PYTHIA.

Chapter 1

Quantum Chromodynamics

1.1 Introduction

An overwhelming variety of subatomic particles were discovered in the latter half of the 20th century. The ever-growing list of particles forced physicists to question their "fundamentality". In 1948 Fermi and Yang were the first to consider pions not as elementary particles, but rather as bound states of nucleon-antinucleon pairs [11]. Although the hypothesis was not confirmed by subsequent experiments, the idea that some particles may be composite did not die.

Symmetries played an integral part in revealing the inner structure of hadrons [12]. The lightest known hadrons can be grouped in groups of ten (decuplet) or eight (octet) according to their spins, parities and mass as seen on Figure 1.1. The particles in each group have identical

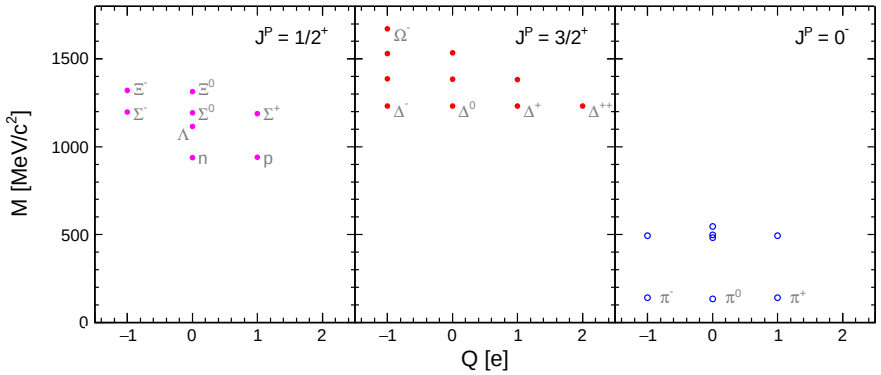

Figure 1.1: Light particles grouped to octets and a decuplet. Particles in each group have similar masses and the same spin and parity.

parity, spins and similar masses[1].

In 1964 Gell-Man and Zweig proposed the explanation for the octet and decuplet arrangement [13]. The octets and decuplets are assumed to be the representations of the $SU(3)$ flavour symmetry group. This means that the particles in each group are the combinations of a fundamental triplet or an antitriplet of the $SU(3)$ group. The proposed explanation implies that

[1] An equivalent structure of the hadron multiplets can be obtained by taking the 3rd isospin component T_3 instead of the electric charge Q and the hypercharge Y instead of the mass M. The relation between Q and T_3 is given by the Gell-Mann–Nishijima equation $Q = T_3 + \frac{Y}{2}$, see [11].

baryons are composed of three fundamental particles— *quarks*. Mesons are composed of a quark-antiquark pair.

Initially only three quarks have been proposed, namely the up, down and strange quarks which are nowadays commonly labelled as u, d, s, respectively. They have been assigned fractions of the elemental charge and a half spin. The model has been very successful in describing many properties of hadrons. For example, it has given an accurate description of the magnetic momenta of various hadrons and thus helped to explain the anomaly that neutral hadrons, such as the neutron, have non-zero magnetic momenta [11]. The mass of the s quark was expected to be larger than the masses of u and d, which causes the break-down of the exact $SU(3)$ symmetry and as a consequence mass splittings in the multiplets is observed. The symmetry between the u and d quarks is much more accurate and results in nearly mass degenerate hadronic states called isospin multiplets.

However, the otherwise successful quark model had some substantial problems. Some of the particles, like the Δ^{++} baryon, were expected to be composed of three identical u quarks with aligned spins. This seems to violate the Pauli exclusion principle which states that two fermions (particles with half integer spins) may not be in the same quantum state. Moreover, isolated individual quarks have never been observed and the theory did not explain what holds the quarks together in hadrons.

These flaws motivated the postulation of an additional degree of freedom later called *the colour charge*. A deeper understanding of the strong interaction was however obtained only after the discovery of *Quantum Chromodynamics (QCD)* , the fundamental theory of the Strong interaction. Its details shall be discussed further.

1.2 Foundations

Let us first examine some mathematical as well a physical concepts needed for the appreciation of QCD. The modern description is based on analytical mechanics, group theory, special relativity, quantum mechanics and relativistic quantum mechanics.

1.2.1 Analytical mechanics

Newtons equations governing classical mechanics are formulated in Cartesian coordinates or any other equivalent coordinate system [14]. This might not be suitable for all systems for constraints may restrict motion in certain directions and thus rendering the mathematical description of the system overly complicated.

One can eliminate the notion of constraints and simplify the mathematical description of the system by using more appropriate coordinate systems. The coordinate systems used in analytical mechanics are called *generalized coordinates*. These coordinate systems are generally curvilinear and their number is equal to the number of degrees of freedom of a system.

Two approaches are commonly used based on the type of generalized coordinates—namely the Lagrangian and Hamiltonian formalisms. Both formalisms are equivalent to Newton's equations [14] and may or may not be more convenient for a given system depending on the particular system modelled.

Let us denote the time derivative of a quantity by a dot over the letter. The Lagrangian formalism uses the generalized coordinates q, the generalized velocities $\dot{q}$ and time to determine the system's configuration. The space of all possible configurations of q and $\dot{q}$ is called *the configuration space*.

Lagrangian formalism is based on the Euler-Lagrange equation

$$\frac{d}{dt}\left(\frac{\partial}{\partial \dot{q}_j}\mathcal{L}(q,\dot{q},t)\right) - \frac{\partial}{\partial q_j}\mathcal{L}(q,\dot{q},t) = 0, \tag{1.1}$$

where $\mathcal{L}(q,\dot{q},t) = T - U$ is a scalar function called the *Lagrangian* and is defined as the kinetic energy minus the potential energy of a system. Note that $\dot{q}$ is an independent variable and is not to be thought of as dependent on q.

The Euler-Lagrange equation may be derived using the *least-action principle*[2] with calculus of variations. Substituting a particular Lagrangian of a system into (1.1) yields the equations of motion.

One can further define a *Lagrangian density* $\mathscr{L}$ as

$$\mathcal{L} = \int_\Gamma \mathscr{L}\, dq, \tag{1.2}$$

where Γ is a region of space.

By applying the Legendre transformation on the variables $(q,\dot{q},t) \to (q,p,t)$ one obtains the Hamiltonian formalism, where $p_i = \frac{\partial \mathcal{L}}{\partial \dot{q}_i}$ is the generalized momentum. These variables are known as canonical variables.

The equations of motion equivalent to (1.1) are

$$\dot{q}_i = \frac{\partial \mathcal{H}}{\partial p_i}, \tag{1.3a}$$

$$\dot{p}_i = -\frac{\partial \mathcal{H}}{\partial q_i}, \tag{1.3b}$$

where $\mathcal{H} = \sum_i p_i\, q_i - \mathcal{L}(q,\dot{q},t)$ is the Hamiltonian. The Hamiltonian is the generalized energy of a system. Note that the first set of equations is equivalent to the definition of momenta and the second set is similar to Newton's equations of motion.

The space of all possible configurations of q and p is called the *phase space*. Note that p is the *generalized* momentum which is a variable independent of q. Therefore p does not have to play the role of momentum in the ordinary sense $\vec{p} = m\vec{v}$, where m is the mass and $\vec{v}$ is the velocity.

Conservation laws and symmetries of the Lagrangian are intimately related. A conserved quantity is a physical observable that does not change during the evolution of a given system. A physical system has a symmetry if there exists a transformation that does not change the system.

Noether's theorem connects conservation laws with symmetries of a system. For example, the conservation of energy arises due to the time symmetry of a system [14]. Symmetries are thus an integral part of analytical mechanics.

1.2.2 Symmetries, groups and transformations

A group $(G,\circ)$ is a set G with a binary operation $\circ$ that satisfies [12]

$$(\forall A,B \in G)\,(A \circ B \in G)\,, \tag{1.4a}$$

$$(\forall A,B,C \in G)\,((A \circ B)\circ C = A \circ (B \circ C))\,, \tag{1.4b}$$

$$(\exists! E \in G)\,(\forall A \in G)\,(A \circ E = E \circ A = A)\,, \tag{1.4c}$$

$$(\forall A \in G)\left(\exists A^{-1} \in G\right)\left(A \circ A^{-1} = A^{-1} \circ A = E\right). \tag{1.4d}$$

[2] The principle of least action states that a function $q(t)$ that makes the action, defined as the time integral of the Lagrangian $\mathcal{S}[q(t)] = \int_{t_1}^{t_2} \mathcal{L}(q,\dot{q},t)dt$, stationary ($\delta\mathcal{S}[q(t)] = 0$) describes the true time evolution of the system. Thus the principle ought to be called the principle of *stationary* action.

An isomorphism $\Phi : G \to \mathbb{C}^{N,N}$ which maps the elements of a group to the space of square $N \times N$ matrices and the operation $\circ$ to matrix multiplication is called the *representation of a group*. The lowest dimensional non-trivial representation of a group is called the *fundamental representation*.

A *Lie group* G is a group whose elements U can be expressed using the matrix exponential

$$U = e^{i\,\alpha_j\,T^j}, \tag{1.5}$$

where $\alpha_i \in \mathbb{C}$ are complex constants and $T^i \in \mathbb{C}^{\mathbb{N},\mathbb{N}}$ are matrices—the *generators* of G [12].

This mathematical construct is appropriate for representing physical transformations. Matrices can be associated with linear operators, which transform a vector.

If a Lagrangian exhibits a symmetry transformation (a transformation that does not change the Lagrangian) a physical quantity is conserved. This fact is formally stated by Noether's theorem. Noether's theorem, in a simplified version, states that

Theorem 1. *(Noether's theorem [14]) For every group of transformations of coordinates $q_j \to q_j = q_j(q, t, \alpha)$, that depends continuously on a parameter $\alpha \in \mathbb{R}$, which leaves the action unchanged, there exists a conserved quantity.*

Integrals of motion (conserved quantities) can greatly simplify the process of solving the equations of motion of a system because they exert constraints on the time evolution. The theorem of Emmy Noether is a very powerful tool that aids the search for solutions to the equations of motion.

Important groups of transformations that shall be further used are the *unitary* group $U(N)$ and the *special unitary* group $SU(N)$, where N is the dimension of the square matrices of the fundamental representation of the groups. The unitary group is a group of complex unitary $N \times N$ matrices whereas $SU(N)$ is a group of unitary $N \times N$ matrices with determinant 1.

1.2.3 Special relativity

Special relativity is based upon the assumptions that the speed of light in vacuum is constant in any reference frame and the laws of physics are invariant in all inertial reference frames. These assumptions lead to a correction of the Galilean transformations. These corrections become sizeable only at speeds close to the speed of light. The corrected transformations are called Lorentz transformations and are a subgroup of the broader Poincaré group which includes translations, rotations and reflections.

The quantity

$$(\Delta s)^2 = c^2\ (\Delta t)^2 - (\Delta x)^2 - (\Delta y)^2 - (\Delta z)^2\,, \tag{1.6}$$

where c is the speed of light, t is time, x, y, z are spatial coordinates and Δ represents the change, is called the *four-interval*. The quantity $(\Delta x)^2 + (\Delta y)^2 + (\Delta z)^2$ is the square of an interval in space while $(\Delta t)^2$ is the square of a time interval. The transformations from the Poincaré group leave the four-interval (1.6) invariant. This allows the combination of space and time in a single entity—*spacetime*. Spacetime is described by the Minkowski space—an analogous vector space to the Euclidean space. A point in spacetime is characterized by the coordinates (ct, x, y, z) and represents the position of a system at a point (x, y, z) in time t (in units scaled by c).

Let us adopt the following notation. Vectors with four components that are elements of the Minkowski space are called four vectors and are denoted by a **bold** face font. Their components are labelled with Greek letters. All three-component vectors are distinguished by an arrow e.g.

$\vec{v}$. Three-component vectors' components are labelled by Latin indices. Therefore Greek indices take values from 0 to 3 and Latin from 1 to 3. Thus a relativistic four-vector is

$$\mathbf{A} = (A^0, \vec{A}) = (A^0, A^1, A^2, A^3), \tag{1.7}$$

and A^μ are components of the four-vector whereas A^i are components of the vector $\vec{A}$. Note that the **bold** face is not used when denoting components A^μ of a four-vector $\mathbf{A}$.

Vectors with upper indices are called *contravariant* and with lower *covariant*.

Contravariant vectors are independent of the change of basis of the vector space. The basis is thought of as the coordinate system, thus contravariant vectors represent vectors in the ordinary sense e.g. velocity. They are transformed by the inverse matrix that transforms the basis of the system making them contra-variant.

Covariant vectors transform with the matrix that transforms the basis of the space. They represent dual vectors (elements of the dual space—a space of linear functionals) e.g. the gradient vector.

A quadratic form

$$\mathbf{A} \cdot \mathbf{B} = \mathbf{A}^T \, g \, \mathbf{B}, \tag{1.8}$$

for two vectors $\mathbf{A}, \mathbf{B}$ from the Minkowski space is defined using the *metric tensor* g.

The time-like metric tensor

$$g = \begin{pmatrix} 1 & 0 & 0 & 0 \\ 0 & -1 & 0 & 0 \\ 0 & 0 & -1 & 0 \\ 0 & 0 & 0 & -1 \end{pmatrix}, \tag{1.9}$$

is used. The quadratic form (1.8) is very similar to an inner product which has an extra property of being positive definite.

A relationship between covariant and contravariant vectors can also be derived using the metric tensor

$$A_\mu = g_{\mu\nu} A^\nu, \tag{1.10}$$

and $g_{\mu\nu} = g^{\mu\nu}$. Note that Einstein's summation convention is in use. It states that if an index is repeated the sum over the index is taken into account $a_i \, b^i = \sum_i a_i \, b^i$. Einstein's summation convention shall be used further.

Using the metric tensor (1.9), the the following relations hold for the quadratic form

$$\mathbf{A} \cdot \mathbf{B} = A^\mu \, B_\mu = A_\mu \, B^\mu = g_{\mu\nu} A^\nu \, B^\mu = A_0 \, B_0 - \vec{A} \cdot \vec{B}, \tag{1.11}$$

where the dot between two vectors $\vec{A} \cdot \vec{B}$ denotes the ordinary inner product.

The quadratic form (1.11) is a quantity invariant under Lorentz transformations. This implies that squaring a four vector (in the sense of the quadratic form $\mathbf{A} \cdot \mathbf{A}$) yields an invariant (as seen in (1.6)).

Important four-vectors are the four-position

$$x^\mu = \left(\frac{t}{c}, \vec{x} \right), \tag{1.12}$$

and the four-momentum

$$p^\mu = \left(\frac{E}{c}, \vec{p} \right). \tag{1.13}$$

Finally, the four-gradient operator is defined in it's contravariant form as

$$\partial^{\mu} := \frac{\partial}{\partial x_{\mu}} = \left(\frac{1}{c}\frac{\partial}{\partial t}, -\vec{\nabla}\right), \tag{1.14}$$

where $\vec{\nabla}$ is the *del* operator, $\vec{\nabla} = \left(\frac{\partial}{\partial x_1}, \frac{\partial}{\partial x_2}, \frac{\partial}{\partial x_3}\right)$, represented by the *nabla* symbol ∇.

1.2.4 Quantum Mechanics

Quantum mechanics describes the behaviour of microscopic systems such as particles. Although it also applies to macroscopic objects, the corrections it introduces to classical physics for macroscopic objects are negligible.

There is a fundamental difference between classical and quantum mechanics. Every measurement (observation) carried out on a quantum mechanical system affects the system. Furthermore, certain physical quantities (e.g. the energy of a bound system) are quantized.

A complex separable Hilbert space[3] $\mathscr{H}$, called the *state space*, is associated with every quantum mechanical system [15]. Every state of a quantum mechanical system is associated with a *ray* (a one-dimensional subset) in $\mathscr{H}$ [15]. A ray Ψ is generated by a unit vector $\psi \in \mathscr{H}$, $\Psi = \{\alpha\psi | \alpha \in \mathbb{C}\}$.

A hermitian[4] operator is associated with every observable of the system [15]. The possible values of measured quantities then correspond to the spectrum of the hermitian operator. Hermitian operators have real spectra implying that the measured observables are real numbers.

Measurements in quantum mechanics have a probabilistic character. The expectation value of an observable that has the operator $\hat{\phi}$ assigned to it is $< \hat{\phi} >_{\psi} = (\psi, \hat{\phi}\psi)$, where $(\bullet, \bullet)$ is the inner product of $\mathscr{H}$ and ψ is a normalized vector in $\mathscr{H}$ that generates the state of the system [15].

The quantum mechanical state of the system $\Psi(\vec{x}, t)$ (also called the *wavefunction*) is not an observable. However, Born's interpretation of quantum mechanics states that $||\psi(\vec{x}, t)||^2$, where $||\bullet||$ is the norm induced by the inner product of $\mathscr{H}$, corresponds to the probability density of finding the system at the position $\vec{x}$ in time t.

The operators corresponding to the position q, momentum p and energy E are defined as

$$\hat{Q}_j\psi := x_j\,\psi, \tag{1.15a}$$

$$\hat{P}_j\psi := -i\hbar\frac{\partial\psi}{\partial x_j}, \tag{1.15b}$$

$$\hat{E}\psi := i\hbar\frac{\partial\psi}{\partial t}, \tag{1.15c}$$

respectively. Note that a hat is used to indicate operators.

The time evolution of a quantum system is described by the Schrödinger equation

$$i\hbar\frac{\partial}{\partial t}\psi\left(\vec{x}, t\right) = \hat{\mathcal{H}}\psi\left(\vec{x}, t\right), \tag{1.16}$$

[3] A complex *Hilbert space* $\mathscr{H}$ is a complex vector space with an inner product that is complete, meaning that every Cauchy sequence $\{x_i\}_{i=0}^{\infty}$ in $\mathscr{H}$ has a limit in $\mathscr{H}$. A Cauchy sequence is a sequence that satisfies $(\forall\varepsilon > 0)\,(\exists n_{\varepsilon})\,(\forall m, n > n_{\varepsilon})\,(\rho(x_n, x_m) < \varepsilon)$ where $\rho(\bullet, \bullet)$ is the metric induced by the inner product. A metric space is separable when it contains a countable everywhere dense subset. A subset $M \subset \mathscr{H}$ is everywhere dense if $\overline{M} = \mathscr{H}$, where $\overline{M}$ is the closure of M [15].

[4] A hermitian operator on $\mathscr{H}$ [15] is an operator (a mapping $\hat{\phi} : \mathscr{H} \to \mathscr{H}$) that satisfies $(\hat{\phi}x, y) = (x, \hat{\phi}y)$ for all $x, y \in \mathscr{H}$, where $(\bullet, \bullet)$ is the inner product of $\mathscr{H}$.

where $\hat{\mathcal{H}}$ is the Hamiltonian operator. For a single particle in a potential $\hat{V}(\vec{x})$ the Hamiltonian is $\hat{\mathcal{H}} = -\frac{\hbar^2}{2m}\hat{\nabla}^2 + \hat{V}(\vec{x})$, where $\hat{\nabla}^2 = \left(\frac{\partial^2}{\partial x^2}, \frac{\partial^2}{\partial y^2}, \frac{\partial^2}{\partial z^2}\right)$ is the Laplacian operator.

1.2.5 Relativistic quantum mechanics

The Schrödinger equation is not invariant under the Lorentz transformations, which is apparent from the fact that for a single particle in a potential $\hat{V}(\vec{x})$ it treats time and space with different orders of differentiation. In order to derive a relativistic version of the Schrödinger equation, consider the following construction.

Suppose the invariant of the four-momentum (1.13)

$$\frac{E^2}{c^2} - p^2 = m^2\, c^2, \tag{1.17}$$

where m is the rest (invariant) mass of a particle. Substituting the observables E and p for their quantum mechanical operator versions one obtains the equation

$$\left(-\frac{1}{c^2}\frac{\partial^2}{\partial t^2} + \hat{\nabla}^2\right)\psi = \frac{m^2\, c^2}{\hbar^2}\psi. \tag{1.18}$$

Equation (1.18) is called the *Klein-Gordon equation*. It is a *second order* equation, therefore it is necessary to specify two initial conditions (for ψ and $\frac{\partial\psi}{\partial t}$) in order to obtain particular solutions. The initial conditions may be specified arbitrarily, hence $||\psi(\vec{x},t)||^2$ can no longer represent the probability of finding the system at $\vec{x}$ in time t. Thus a first order equation is desired.

Therefore Dirac proposed the following decomposition of the left hand size. The operator on the left hand side of (1.18) is decomposed into it's "square roots"

$$-\frac{1}{c^2}\frac{\partial^2}{\partial t^2} + \hat{\nabla}^2 = \left(A\frac{\partial}{\partial x_1} + B\frac{\partial}{\partial x_2} + C\frac{\partial}{\partial x_3} + \frac{i}{c}D\frac{\partial}{\partial t}\right)^2. \tag{1.19}$$

In order for the cross terms $\left(\text{e.g. } \frac{\partial}{\partial x_1}\frac{\partial}{\partial x_2}\right)$ in (1.19) to vanish, the coefficients must satisfy $AB + BA = 0$, $AC + CA = 0$ etc. However since the square terms must have unit coefficients, $A^2 = 1$ and $B^2 = 1$ must also hold.

These conditions determine that the objects A, B, C and D cannot be ordinary complex numbers. One possibility is to consider A, B, C and D to be 4×4 *matrices*[5]. This implies that the wavefunction ψ has four components. The first order equation obtained by taking the "square root" of (1.18) is the Dirac equation

$$i\hbar\gamma^\mu\partial_\mu\psi - mc\psi = 0, \tag{1.20}$$

where γ^μ are four matrices

$$\gamma^0 = \begin{pmatrix} 1 & 0 & 0 & 0 \\ 0 & 1 & 0 & 0 \\ 0 & 0 & -1 & 0 \\ 0 & 0 & 0 & -1 \end{pmatrix},\ \gamma^1 = \begin{pmatrix} 0 & 0 & 0 & 1 \\ 0 & 0 & 1 & 0 \\ 0 & -1 & 0 & 0 \\ -1 & 0 & 0 & 0 \end{pmatrix},$$
$$\gamma^2 = \begin{pmatrix} 0 & 0 & 0 & -i \\ 0 & 0 & i & 0 \\ 0 & i & 0 & 0 \\ -i & 0 & 0 & 0 \end{pmatrix},\ \gamma^3 = \begin{pmatrix} 0 & 0 & 1 & 0 \\ 0 & 0 & 0 & -1 \\ -1 & 0 & 0 & 0 \\ 0 & 1 & 0 & 0 \end{pmatrix}, \tag{1.21a}$$

[5] Another approach uses *quaternions* which is a non-commutative extension to complex numbers that has three distinct imaginary units [16].

obtained by solving (1.19). Using the gamma matrices one can define a notation for covariant vectors

$$\not{A} = \gamma^\mu A_\mu, \tag{1.22}$$

known as the Feynman slash notation. Using Feynman's slash notation the Dirac equation becomes

$$\left(i\hbar\not{\partial} - mc\right)\psi = 0. \tag{1.23}$$

The corresponding Lagrangian density to (1.23) is

$$\mathscr{L} = c\,\overline{\psi}\left(i\hbar\not{\partial} - mc\right)\psi, \tag{1.24}$$

where $\overline{\psi}$ is the Dirac adjoint wavefunction defined as $\overline{\psi} := \psi^\dagger\gamma^0$, where $\psi^\dagger$ is the Hermitian conjugate of ψ. The Lagrangian density (1.24) describes a free, half spin particle.

1.2.6 Quantum electrodynamics and guauge invariance

Quantum electrodynamics (QED) is the theory of the electromagnetic interactions at the quantum field theory level. QED is invariant under the local $U(1)$ group of transformation. This according to Noether's theorem results in a quantity being conserved. The conserved quantity in QED is the electric current and thus the electric charge is also conserved. The QED Lagrangian density can be derived from the free Dirac equation (1.24) using the local $U(1)$ symmetry [17].

Suppose a local $U(1)$ transformation of the wavefunction

$$\psi(x)' = U(x)\,\psi(x) = e^{-i\,\alpha(x)}\psi, \tag{1.25a}$$

$$\overline{\psi(x)}' = \overline{\psi(x)}\,U^\dagger(x) = \overline{\psi}\,e^{i\,\alpha(x)}, \tag{1.25b}$$

where $U^\dagger(X)$ is the Hermitian conjugate of $U(x)$, ψ is the solution of the Dirac equation, $\alpha(x)$ is an arbitrary complex function of the space-time coordinate x. The minus sign in (1.25a) is chosen for later convenience. The transformation is local because a $U(1)$ transformation is considered in every space-time point x—hence the dependence of α on x. The local transformation (1.25) is called the *gauge transformation*.

Substituting (1.25) into (1.24) one obtains the transformed Lagrangian

$$\mathscr{L}' = c\overline{\psi}'\left(i\hbar\not{\partial} - mc\right)\psi' = c\overline{\psi}\,e^{i\,\alpha(x)}\left(i\hbar\not{\partial} - mc\right)e^{-i\,\alpha(x)}\psi. \tag{1.26}$$

Applying the product rule for the four-divergence yields

$$\mathscr{L}' = c\overline{\psi}\left(i\hbar\left(\not{\partial} - i\not{\partial}\alpha(x)\right) - mc\right)\psi = c\overline{\psi}\left(i\hbar\not{\partial} - mc\right)\psi + c\hbar\,\overline{\psi}\not{\partial}\alpha(x)\psi. \tag{1.27}$$

The term $-i\not{\partial}\alpha(x)$ spoils the invariance of (1.27). The usual approach of fixing the invariance is as follows. The four-gradient $\not{\partial}$ is replaced by *the gauge-covariant derivative* $\not{D}$ so that $\overline{\psi}\not{D}\psi$ is gauge invariant. With the introduction of a new vector potential $A_\mu(x)$ the gauge-covariant derivative is

$$\not{D} = \not{\partial} + ie\not{A}, \tag{1.28}$$

where the scaling factor e represents the strength of the electromagnetic interaction. Substituting (1.28) for the four-gradient into (1.24) yields

$$\mathscr{L} = c\,\overline{\psi}\left(i\hbar\not{D} - mc\right)\psi = c\,\overline{\psi}\left(i\hbar\left(\not{\partial} + ie\not{A}\right) - mc\right)\psi. \tag{1.29}$$

Performing the gauge $U(1)$ transformation (1.25) on (1.29) yields

$$\mathscr{L} = c\,\overline{\psi}\left(i\hbar\left(\partial\!\!\!/ - i\partial\!\!\!/\alpha(x) + ieA\!\!\!/'\right) - mc\right)\psi, \tag{1.30}$$

where $A\!\!\!/' = U^{\dagger}(x)A\!\!\!/U(x)$. In order to make (1.30) gauge invariant, the A_μ field must transform as

$$A'_\mu = A_\mu + \frac{1}{e}\partial_\mu\alpha(x). \tag{1.31}$$

To make the gauge field A_μ a dynamical variable, a term involving the derivatives of A_μ is added to the Lagrangian. This term needs to be gauge-invariant. This is achieved by defining the *electromagnetic field strength tensor* as

$$F_{\mu\nu} = \partial_\mu A_\nu - \partial_\nu A_\mu. \tag{1.32}$$

Substituting (1.31) into (1.32) leads to

$$F'_{\mu\nu} = \partial_\mu\left(A_\nu + \frac{1}{e}\partial_\nu\alpha(x)\right) - \partial_\nu\left(A_\mu + \frac{1}{e}\partial_\mu\alpha(x)\right) = \partial_\mu A_\nu - \partial_\nu A_\mu = F_{\mu\nu}, \tag{1.33}$$

where $F'_{\mu\nu}$ is the transformed electromagnetic field strength tensor. The covariant derivatives in (1.33) have been interchanging thus imposing a condition of continuity[6] on the second derivatives of A_μ.

To summarize, the locally $U(1)$ invariant Lagrangian density of QED is

$$\mathscr{L}_{QED} = c\,\overline{\psi}\left(i\hbar D\!\!\!/ - mc\right)\psi - \frac{1}{4}F_{\mu\nu}F^{\mu\nu}, \tag{1.34}$$

where the covariant derivative is

$$D\!\!\!/ = \partial\!\!\!/ + ieA\!\!\!/, \tag{1.35}$$

the gauge transformation is

$$A_\mu \to A_\mu + \frac{1}{e}\partial_\mu\alpha, \tag{1.36}$$

and the electromagnetic field strength tensor is defined as

$$F_{\mu\nu} = \partial_\mu A_\nu - \partial_\nu A_\mu. \tag{1.37}$$

Note that the factor of $\frac{1}{4}$ comes from the normalization of the kinetic energy in the equations of motion derived from the Lagrangian density.

1.3 Quantum Chromodynamics

Quantum Chromodynamics (QCD) is the theory describing the strong interaction. QCD can be derived from the free Dirac field similarly to QED.

Experimental evidence from deep inelastic scattering at SLAC suggested that quarks inside a proton are loosely bound [19]. This implies that QCD describing quarks must be an *asymptotically free* theory, meaning that quarks behave as free particles when they are close together.

[6] If both second partial derivatives $\frac{\partial^2 f(x,y)}{\partial x \partial y}$ and $\frac{\partial^2 f(x,y)}{\partial y \partial x}$ of a function $f(x,y)$ are continuous, then $\frac{\partial^2 f(x,y)}{\partial x \partial y} = \frac{\partial^2 f(x,y)}{\partial y \partial x}$, see [18].

One can show that only Yang-Mills theories (theories invariant under $SU(N)$ transformations) can produce asymptotic freedom [17]. Another piece of experimental evidence suggests that there are *three* charges in the strong interaction as opposed to one charge in QED. This suggests setting $N = 3$ making QCD invariant under $SU(3)$ transformations [12]. The charges are labelled *red*, *green* and *blue* for convenience. A neutral composite object has white colour. Note that this is a different $SU(3)$ group of transformations as the one mentioned in the introduction describing the *flavour* symmetry of quarks.

Similarly to (1.25), consider the local $SU(3)$ transformation given by

$$U(x) = e^{-i\beta^a(x)\frac{\lambda_a}{2}}, \tag{1.38}$$

where λ_a are the Gell-Mann matrices

$$\begin{aligned}
\lambda_1 &= \begin{pmatrix} 0 & 1 & 0 \\ 1 & 0 & 0 \\ 0 & 0 & 0 \end{pmatrix}, \ \lambda_2 = \begin{pmatrix} 0 & -i & 0 \\ i & 0 & 0 \\ 0 & 0 & 0 \end{pmatrix}, \ \lambda_3 = \begin{pmatrix} 1 & 0 & 0 \\ 0 & -1 & 0 \\ 0 & 0 & 0 \end{pmatrix}, \ \lambda_4 = \begin{pmatrix} 0 & 0 & 1 \\ 0 & 0 & 0 \\ 1 & 0 & 0 \end{pmatrix}, \\
\lambda_5 &= \begin{pmatrix} 0 & 0 & -i \\ 0 & 0 & 0 \\ i & 0 & 0 \end{pmatrix}, \ \lambda_6 = \begin{pmatrix} 0 & 0 & 0 \\ 0 & 0 & 1 \\ 0 & 1 & 0 \end{pmatrix}, \ \lambda_7 = \begin{pmatrix} 0 & 0 & 0 \\ 0 & 0 & -i \\ 0 & i & 0 \end{pmatrix}, \ \lambda_8 = \frac{1}{\sqrt{3}} \begin{pmatrix} 0 & 0 & 0 \\ 0 & 1 & 0 \\ 0 & 0 & -2 \end{pmatrix},
\end{aligned} \tag{1.39a}$$

and $\frac{\lambda_a}{2}$ form the fundamental representation of $SU(3)$. Let $t_a = \frac{\lambda_a}{2}$ for convenience.

Similarly to QED, a vector potential is introduced to make the Lagrangian gauge invariant. In this case, there are eight terms and thus eight vector potentials A^a_μ, $a = 1 \dots 8$, are needed.

The gauge-covariant derivative is then defined as

$$D_\mu := \partial_\mu + i\, g_{QCD} A^a_\mu\, t_a, \tag{1.40}$$

where g_{QCD} represents the coupling strength.

The non-Abelian (non-commutative) nature of the group $SU(3)$ introduces a significant difference between QCD and QED. The QCD Lagrangian density is not invariant under the QED gauge potential transformation

$$A^a_\mu \to A^a_\mu + \frac{1}{g_{QCD}} \partial_\mu \beta^a(x), \tag{1.41}$$

and other terms are needed.

In order to derive the correction on (1.41), infinitesimal transformations

$$\psi' = e^{-i\beta^a(x)\frac{\lambda_a}{2}} \psi \approx \left(1 - i\beta^a(x)\frac{\lambda_a}{2}\right) \psi, \tag{1.42a}$$

$$\overline{\psi}' = \overline{\psi} e^{i\beta^a(x)\frac{\lambda_a}{2}} \approx \overline{\psi} \left(1 + i\beta^a(x)\frac{\lambda_a}{2}\right), \tag{1.42b}$$

are considered where a Taylor series expansion has been used on (1.38) and only terms up to linear in $\beta^a(x)$ have been kept.

Substituting the transformations into the Dirac Lagrangian density yields a transformed Lagrangian density

$$\mathscr{L}' = c\, \overline{\psi}' \left(i\hbar \not{D} - mc\right) \psi' = c\, \overline{\psi}' \left(i\hbar \left(\not{\partial} + ig t_a \not{A}^a\right) - mc\right) \psi'. \tag{1.43}$$

The four-gradient $\not{\partial}$ transforms analogously to the QED case. To explore the correction on (1.41), the term

$$ig\,\overline{\psi}' t_a \gamma^\mu \psi'\, A^a_\mu, \tag{1.44}$$

is examined closer. Substituting the infinitesimal transformations (1.42) into (1.44) and expanding leads to

$$ig\,\overline{\psi}\left(t_a + i\beta^b(x) t_a t_b - i\beta^b(x) t_b t_a\right)\gamma^\mu \psi\, A^a_\mu, \tag{1.45}$$

where a new summation variable b has been introduced and a term proportional to the square of β^b has been ignored due to infinitesimal transformations. Equation (1.45) can be rewritten using the commutator operator $[\bullet, \bullet]$ as

$$ig\,\overline{\psi}\left(t_a + i\beta^b(x)\,[t_a, t_b]\right)\gamma^\mu \psi\, A^a_\mu. \tag{1.46}$$

The commutator term can be expressed as

$$[t_a, t_b] = i\, f^{abc} t_c \tag{1.47}$$

where f^{abc} are the structure constants of the $SU(3)$ group [12] and are numerically $f^{123} = 1$, $f^{147} = -f^{156} = f^{246} = f^{257} = f^{345} = -f^{367} = \frac{1}{2}$ and $f^{458} = f^{678} = \frac{\sqrt{3}}{2}$. Equation (1.46) then becomes

$$ig\,\overline{\psi}\left(t_a - \beta^b(x) f^{abc} t_c\right)\psi\, \not{A}^a. \tag{1.48}$$

This implies that the vector potential should have a term proportional to $\beta^b(x) f^{abc}$ in it's transformation to render the Lagrangian density invariant.

The infinitesimal gauge transformation of the vector potential of QCD is therefore

$$A^a_\mu \to A^a_\mu + \frac{1}{g_{QCD}}\partial_\mu \beta^a(x) + \beta^b(x) f^{abc} A^c_\mu. \tag{1.49}$$

The Lagrangian density describing quarks (for one flavour) including their interaction with the gluon potentials is

$$\mathscr{L}_q = c\,\overline{\psi}\left(i\hbar \not{D} - mc\right)\psi, \tag{1.50}$$

The gluons are represented as an antisymmetric field strength tensor $G^a_{\mu\nu}$ similarly to $F_{\mu\nu}$ in QED. The gluon field strength tensor [11] is defined with the help of the gauge covariant derivative as follows

$$G^a_{\mu\nu} t_a = \frac{1}{ig_{QCD}}\left[D_\mu, D_\nu\right]. \tag{1.51}$$

Substituting (1.40) into (1.51) yields

$$[D_\mu, D_\nu] = \left(\partial_\mu + ig_{QCD} A^a_\mu t_a\right)\left(\partial_\nu + ig_{QCD} A^a_\nu t_a\right) - \left(\partial_\nu + ig_{QCD} A^a_\nu t_a\right)\left(\partial_\mu + ig_{QCD} A^a_\mu t_a\right). \tag{1.52}$$

Expanding the terms, using the properties of the commutator and introducing a new summation variable b leads to

$$[D_\mu, D_\nu] = ig_{QCD}\left(\partial_\mu A^a_\nu t_a - \partial_\nu A^a_\mu t_a\right) + g^2_{QCD}\,[t_a, t_b]\, A^a_\mu A^b_\nu, \tag{1.53}$$

the second term can be rewritten using (1.47) and introducing a new summation variable c as

$$g^2_{QCD}\,[t_a, t_b]\, A^a_\mu A^b_\nu = ig^2_{QCD} f^{abc} t_c A^a_\mu A^b_\nu = -ig^2_{QCD} f^{abc} t_a A^b_\mu A^c_\nu, \tag{1.54}$$

where the summation indices have been relabelled and the antisymmetry of the structure constant has been exploited.

Equations (1.51), (1.54) and (1.53) imply an equivalent definition of the gluon field strength tensor

$$G^a_{\mu\nu} = \partial_\mu A^a_\nu - \partial_\nu A^a_\mu - g_{QCD}\, f^{abc} A^b_\mu A^c_\nu, \tag{1.55}$$

where $a, b, c = 1 \ldots 8$ are colour indices.

The gluon field strength tensor transforms non-trivially as opposed to the electromagnetic field strength tensor of QED. This is due to the third term in (1.55), which causes a possibility of direct coupling among gluons [11].

The gauge invariance of (1.55) can be proven based on the examination of the trace operator. Consider the transformations (1.38) on $G^a_{\mu\nu}$ in the trace operator

$$\mathrm{Tr}\left(G^a_{\mu\nu}{}' t_a G^{\mu\nu\prime}_b t_b\right) = \mathrm{Tr}\left(U^{-1} G^a_{\mu\nu} t_a U U^{-1} G^{\mu\nu}_b t_b U\right) = \mathrm{Tr}\left(G^a_{\mu\nu} t_a G^{\mu\nu}_b t_b\right), \tag{1.56}$$

where the commutativity of the trace operator has been used. Equation (1.56) verifies that the term $\mathrm{Tr}\left(G^a_{\mu\nu} t_a G^{\mu\nu}_b t_b\right)$ is gauge invariant. Using the obvious property of the Gell-Mann matrices, $\mathrm{Tr}(t_a t_b) = \frac{1}{2}\delta_{a,b}$, the trace of the gluon field strengths tensors is

$$\mathrm{Tr}\left(G^a_{\mu\nu} t_a G^{\mu\nu}_b t_b\right) = \mathrm{Tr}(t_a\, t_b) G^a_{\mu\nu} G^{\mu\nu}_a = \frac{1}{2}\delta_{a,b} G^a_{\mu\nu} G^{\mu\nu}_b = \frac{1}{2} G^a_{\mu\nu} G^{\mu\nu}_a, \tag{1.57}$$

verifying that the term $G^a_{\mu\nu} G^{\mu\nu}_a$ is gauge invariant.

The Lagrangian density describing gluon fields is, similarly to QED,

$$\mathscr{L}_g = -\frac{1}{4} G^a_{\mu\nu} G^{\mu\nu}_a. \tag{1.58}$$

The QCD Lagrangian density is then the sum of the individual Lagrangian densities describing quarks and gluons

$$\mathscr{L}_{QCD} = \mathscr{L}_q + \mathscr{L}_g = \sum_{\text{flavour}} c\,\overline{\psi}\left(i\hbar \not{D} - mc\right)\psi - \frac{1}{4} G^a_{\mu\nu} G^{\mu\nu}_a, \tag{1.59}$$

where

$$D_\mu := \partial_\mu + i\, g_{QCD} A^a_\mu\, t_a, \tag{1.60}$$

is the gauge covariant derivative of QCD and the infinitesimal transformation of the gluon field is

$$A^a_\mu \to A^a_\mu + \frac{1}{g_{QCD}} \partial_\mu \beta^a(x) + \beta^b(x) f^{abc} A^c_\mu, \tag{1.61}$$

and the gluon field strength tensor is

$$G^a_{\mu\nu} = \partial_\mu A^a_\nu - \partial_\nu A^a_\mu - g_{QCD}\, f^{abc} A^b_\mu A^c_\nu. \tag{1.62}$$

1.4 Quarks, gluons and the strong interaction

As stated in the introductory chapter, QCD describes the Strong interaction—one of the four fundamental interactions of nature. The fact that there are eight generators of the $SU(3)$ group (the Gell-Mann matrices), mandating the introduction of eight gauge vector potentials A^a_μ and

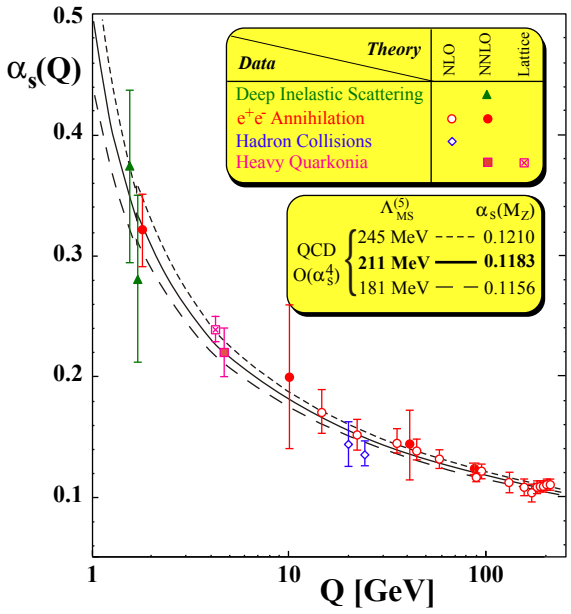

Figure 1.2: The running of the QCD coupling constant [20].

eight gluon field strength tensors $G^a_{\mu\nu}$, implies the existence of *eight* different types of gluons—the particles mediating the strong force. On the other hand, the group $U(1)$ describing QED has only one generator and postulates only one vector potential for the photon. Note that both photons and gluons are massless for the term $A_\mu A^\mu$ (or $A^a_\mu A^\mu_a$ in QCD) is not gauge invariant. Also, the photon field does not couple to itself whereas the gluon field does. This is because the photon does not carry the electromagnetic charge [17].

The strength of the Strong interaction is related to the size of the coupling constant α_s which is proportional to the QCD gauge coupling constant g_{QCD} as

$$\alpha_s = \frac{g^2_{QCD}}{4\pi}. \tag{1.63}$$

Let Q^2 be the square of the momentum transfer of a collision. The coupling constant α_s is not a constant. As follows from perturbation theory, α_s is running. This means that as $Q^2 \to \infty$, α_s vanishes yielding a non-interaction theory (asymptotic freedom). On the other hand, as $Q^2 \to 0$, α_s grows to infinity. It is believed that this behaviour of α_s causes colour confinement (colour charges are confined into colourless hadrons). The behaviour of α_s obtained from experiments and calculated from theory is shown in Figure 1.2.

1.5 QCD predictions

The Quark-parton model (QPM) [11] can, together with QCD, describe any hard (governed by short distance interactions) collision of two particles A and B of the scheme

$$A + B \to F, \tag{1.64}$$

where F is an unspecified final state. The particles A and B may in principle be any hadrons, leptons or gauge bosons [11]. Leptons and gauge bosons are considered elementary and thus

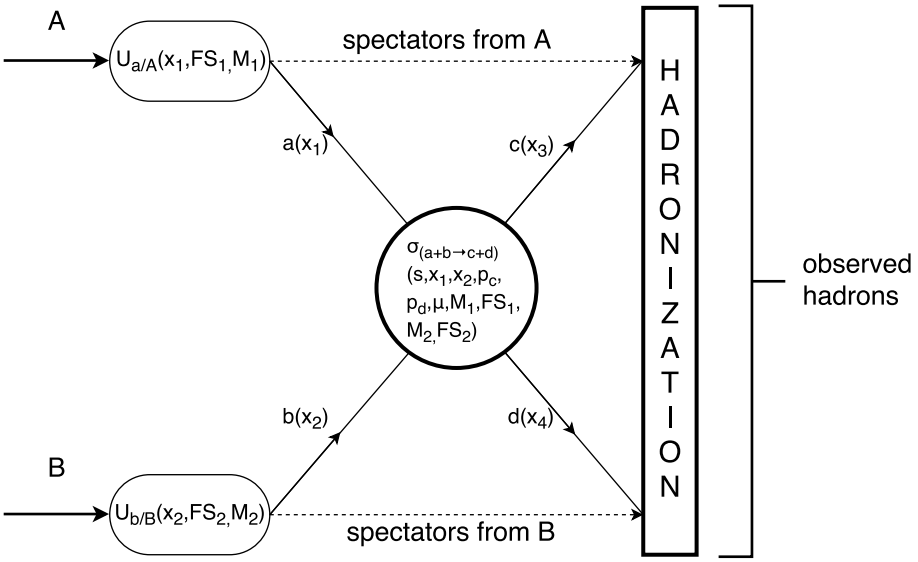

Figure 1.3: The general scheme of QCD improved QPM [11].

coincide with their constituents. The process can be divided into three distinct levels as seen in Figure 1.3.

1. First, the initial evolution is governed by the *parton distribution functions (PDFs)* $U_{a/A}(x_1, FS_1, M_1)$ and $U_{b/B}(x_2, FS_2, M_2)$. PDFs describe the distribution of partons, bosons or leptons a, b in the beam particles A and B that are undergoing a hard scattering process. PDFs depend on the momentum fraction (the fraction of the initial momentum) x_i and on the factorization scheme FS_i and factorization scale M_i.

   PDFs are phenomenological quantities and cannot yet be obtained from the first principles of QCD. They were obtained empirically from data, e.g. from the *deep inelastic scattering (DIS)* of leptons on hadrons. They are therefore strongly dependent on the energy of the leptons in DIS[7]. This is represented by the factorization scheme and scale. However, PDFs are universal, meaning that they can be used in any process involving the given hadron specie and the constituent in the output channel.

   PDFs for leptons and gauge bosons are considered to be Dirac delta functions in a first approximation.

2. The hard scattering of partons a, b producing partons c, d is described by the parton-level cross section $\sigma^{QCD}_{a+b\to c+d}(s, x_1, x_2, p_c, p_d, \mu, M_1, FS_1, M_2, FS_2)$, where s is the square of the centre of mass energy of a and b, p_c and p_d are the four-momenta of c and d, respectively and μ is the hard scattering scale. This cross-section is calculable directly from QCD.

3. Finally, the hadronization is a process where the produced partons c and d restore their colour field equilibrium and become parts of final state hadrons. This stage is also purely phenomenological and is described by the fragmentation function $D_{\mathrm{h/c}}(z, M, FS)$, which is proportional to the probability that the parton c fragments into the hadron h.

[7] The momentum of the lepton is related to a wavelength. The higher the momentum the shorter the wavelength and the probe (the lepton) can distinguish finer structures.

This factorization can be considered under the assumption that the initial and final states of the interaction are much further apart in time than the proper time of the hard scattering process.

One can express the final cross-section of the production of the hadron h in the reaction A + B as

$$\sigma_{A+B\to h+X} = \sum_{a,b,c,d} \int dx_1\, dx_2\, U_{a/A} \cdot U_{b/B} \cdot \sigma^{QCD}_{a+b\to c+d} * D_{\mathrm{h/c}}, \tag{1.65}$$

where the sum runs over all combinations of a, b, c, d that lead to the final state F which involves the hadron h and $*$ signifies further integration over p_c and p_d which lead to the final state F. Note that the final state does not necessarily have to be a particle. One can use (1.65) to calculate the cross-sections of *jets* using a fragmentation function that describes the production of a jet.

1.6 Jets

As previously stated, individual isolated partons have never been observed due to the colour confinement. Hence a parton that underwent a hard scattering process tends to restore it's colour field equilibrium configuration. It does so by radiating partons—*parton showering*. These collimated, high energy parton showers are called *jets*.

A jet might not be an obvious structure when looked upon by eye and a rigorous definition of the concept is therefore needed. Jets are intuitively understood as collimated showers of particles coming from a fragmentation process. Rigorous definition of a jet is however based on the algorithms which are going to be discussed in detail in the next section [21].

Jets are used in many areas of physics analyses and may help in understanding various properties of the top quark, hadronisation, hadron structure, quark gluon plasma and others.

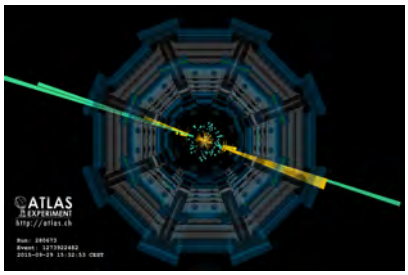

Figure 1.4: A two jet event as seen by ATLAS [22].

Chapter 2

Jet algorithms

2.1 Introduction

In order to extract relevant information about the jets from the data acquired during a particle collision, a definition of a jet via a *jet algorithm* is needed. A jet is a phenomenological concept that provides a well defined link between theory and experiment when we attempt to get a proxy for description of properties of partons that underwent hard scattering.

Using the aforementioned jet definition, a jet algorithm can recombine the lost energy in parton showering and yield the desired information. The algorithm takes final-state particles as the input and determines a "distance" between particles. It groups particles into jets by applying certain criteria (depending on the specific algorithm) to the distance.

2.2 Jet algorithms

A jet algorithm is a set of laws by which the algorithm groups different particles and assigns them a resulting four-momentum vector. Hence a definition of a distance metric is necessary. A jet algorithm should satisfy obvious conditions such as simplicity of implementation in both theoretical and experimental cases and should yield finite cross sections as well as be independent of the order of perturbation theory [23]. In general, it is possible to divide jet algorithms into two distinct approaches deemed "top-down" and "bottom-up".

2.2.1 Cone algorithms

The first of these approaches, the so called "top-down" approach, is based on clustering particles into angular cones. Historically the first Cone algorithm classified an event as having two jets if at least a fraction of the total energy $1 - \varepsilon$ has been contained in two cones having an opening angle δ. This approach had two parameters ε and δ introducing some measure of arbitrariness.

The cone algorithms have evolved substantially since 1970. Most cone algorithms use an iterative approach by choosing a particle which defines a direction and computing the sum of the momenta of all particles in an angular cone of a radius R around the particle in the azimuth and rapidity. The resulting direction of the summed momenta defines a new direction. This procedure is repeated until the jet is stable. The parameter R is known as the jet radius [23].

A problem arises when two neighbouring jets overlap. A variety of different approaches might be used to resolve this problem. One way is to take the hardest particle as the seed, form a jet

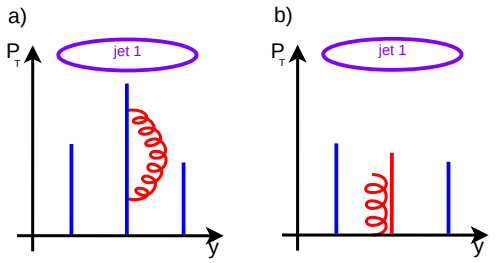

Figure 2.1: Collinearly safe algorithms.

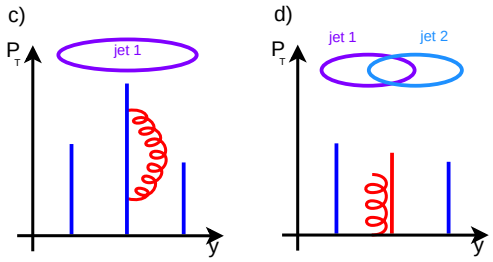

Figure 2.2: Collinearly unsafe algorithms.

around it by the iterative method and remove all the particles from the newly-formed jet from the event and repeat this procedure until no particles are left. This method eliminates the issue that has arisen with overlapping jets.

A different approach called the split-merge procedure may be used. This method finds all stable cones in the event and if two cones overlap it either merges the two jets into one or splits the particles. It merges the two jets if one has more than a fraction f of it's transverse momentum in the particles shared. Otherwise it splits the particles and assigns them to the two jets by distance.

Cone algorithms are mentioned solely for historical purposes. They generally (except the SISCone algorithm) do not meet infrared and collinear safety which shall be discussed in the next section.

2.2.2 Infrared and collinear safety

Infrared and collinear (IRC) safety are important properties of a jet algorithm that ensure the satisfaction of a finite jet production cross section. Infrared safety signifies that a jet configuration in an event does not change by an addition of an infinitesimally soft particle. This is especially important for the algorithm's independence on the degree of perturbation theory.

Collinear safety conveys the independence of a jet configuration on collinear splittings of particles.

Both soft emissions and collinear splittings are associated with divergent matrix elements in the respective perturbative theory. IRC unsafe jets may prevent a cancellation of divergences that appear in the perturbative series in tree-level and loop diagrams. These two sources of jets then do not cancel which leads to an infinite cross-section. Therefore the IRC safety is imperative in any jet algorithm.

The aforementioned cone algorithms suffer greatly from IRC unsafety and are therefore rendered inappropriate.

2.2.3 Sequential recombination algorithms

A sequential recombination algorithm uses a metric to decide whether to merge particles into a jet. The definition of the metric depends on the specific algorithm used. A simple sequential recombination algorithm goes as follows.

1. A metric $\rho(i, j)$ (distance) between each pair of particles i and j is computed.

2. The minimum of $\rho(i, j)$ is found.

3. If the minimum distance is less than a certain threshold ρ_{cut} the two particles are merged into a single particle called a *pseudojet*. And the procedure is repeated from step 1.

4. Otherwise all remaining particles and/or pseudojets are declared as jets and the iteration is terminated.

This approach yields an algorithm that is IRC safe because both soft emissions and collinear splittings are recombined into a pseudojet [23].

2.2.3.1 The k_t algorithm

e^+e^- collisions

Considering e^+e^- collisions, one can define a metric as

$$\rho(i,j) = \frac{2\min(E_i^2, E_j^2)\,(1-\cos\theta_{ij})}{Q^2}, \tag{2.1}$$

where E_i is the energy of the i-th particle, θ_{ij} the angle between the i-th and j-th particle and Q is the total energy in the event.

The issue of soft back-to-back particle recombination might arise with different metrics. A pair of two very soft particles which are back-to-back might have a smaller distance than a soft particle which is close in angle to a hard particle. The choice of metric (2.1) (namely the use of min()) avoids this problem [23].

Hadron collisions

When colliding hadrons as opposed to e^+e^- two issues arise. Firstly the total energy in an event Q is ill-defined. Secondly the divergences in the QCD branching probability are no longer restricted to pairs of outgoing particles but also arise amongst an outgoing particle and the direction of the incoming beam. One can define a dimensionful metric by substituting the parameter Q by a parameter R that closely resembles the "jet radius" from cone algorithms. Furthermore, it is convenient to use metrics that are invariant under longitudinal Lorentz boosts.

The following metrics are used in the k_t algorithm for hadron collisions

$$d_{ij} = \min(p_{T\,i}^2, p_{T\,j}^2)\frac{\Delta R_{ij}^2}{R^2}, \qquad \Delta R_{ij}^2 = (y_i - y_j)^2 + (\phi_i - \phi_j)^2\,, \tag{2.2a}$$

$$d_{iB} = p_{T\,i}^2, \tag{2.2b}$$

where p_T, y and ϕ are the transverse momentum, rapidity and the azimuthal angle, respectively. The quantity R is analogous to the jet radius used in cone algorithms.

Both metrics are longitudinally invariant since both p_T^2 and ΔR^2 are invariant under longitudinal Lorentz Boosts. The general sequential recombination algorithm is then modified for the k_t algorithm as follows:

1. Find all the relevant distances (2.2a) and (2.2b).

2. Find the minimum of all (2.2a) and (2.2b).

3. If it is (2.2a) combine i and j into a *pseudojet* and return to step 1.

4. If it is (2.2b) declare the pseudojet (or particle) i as a final state jet and remove it from the list and go to step 1.

5. If no pseudojets or particles remain, terminate the iteration.

The definition of metric (2.2a) prefers clustering softer particles rather than hard ones. Hence the k_t algorithm is appropriate for underlying event reconstruction and subsequent background subtraction. The resulting jets from the k_t algorithm are often of irregular shape [23].

2.2.3.2 The *anti-*k_t algorithm

If one prefers hard particle clustering rather than a soft one, a metric redefinition is needed. When negative powers of p_T are used the aforementioned goal is achieved. Thus the metric definition [23]

$$d_{ij} = \min(p_{T\,i}^{-2}, p_{T\,j}^{-2}) \frac{\Delta R_{ij}^2}{R^2}, \qquad \Delta R_{ij}^2 = (y_i - y_j)^2 + (\phi_i - \phi_j)^2 \,, \tag{2.3a}$$

$$d_{iB} = p_{T\,i}^{-2}, \tag{2.3b}$$

is used in an algorithm known as the *anti-*k_t algorithm. The *anti-*k_t algorithm grows a jet "outwards" around hard seed particles. This results in jets which are more circular than those obtained from the k_t algorithm. The *anti-*k_t is IRC safe too.

The most widely used algorithm is the *anti-*k_t. The k_t algorithm is then used for background subtraction. The comparison of jets clustered by the k_t and anti-k_t algorithms is demonstrated

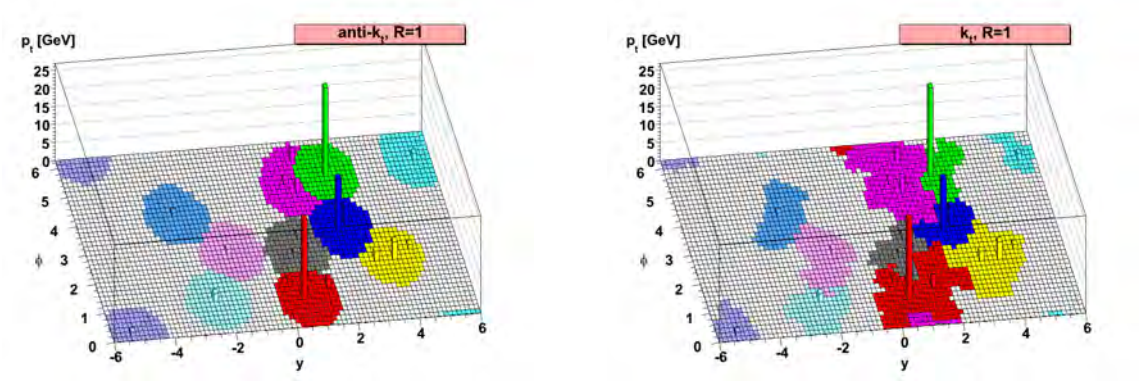

Figure 2.3: The y-ϕ distribution of jets clustered by the anti-k_t algorithm (left) and the k_t algorithm (right) [23].

in Figure 2.3.

2.2.4 Implementation

In the first step of the k_t algorithm a particle is chosen and the distance to every other particle is computed. This is done for all the particles. Hence the complexity of k_t is $\mathcal{O}(N^3)$. The complexity rendered the k_t (as well as the *anti-*k_t) inappropriate for speed reasons and cone algorithms have been preferred. In 2005 FastJet came with a fast implementation of k_t that reduced the complexity to $\mathcal{O}(N \ln N)$. This reduction of complexity lead to the widespread adoption of the anti-k_t algorithm.

Chapter 3

Unfolding

3.1 Introduction

In experiments, jets are reconstructed from particles measured by a detector. The jet spectra are therefore affected by various detector effects e.g. inaccurate energy and momentum measurements, the particle reconstruction efficiency etc. Thus corrections of the measured spectra on these detector effects are necessary. The corrections are usually carried out by unfolding.

Suppose that a vector $\vec{b}^{rec}$ represents a distribution of a physical quantity reconstructed by the detector. If the spectrum is in the form of an histogram, $\vec{b}^{rec}$ corresponds to the bin content of individual bins. It is desired to obtain the distribution of the true, detector-unaffected physical quantity $\vec{b}^{true}$. A linear relation of true and measured distributions is often expected. This linear transformation is described by the so-called response matrix $\mathbb{A}$ of the detector which is usually acquired by means of Monte Carlo simulations. Hence one has to solve a linear system

$$\mathbb{A}\vec{b}^{true} = \vec{b}^{rec}. \tag{3.1}$$

Thus the elements of the response matrix represent *probabilities* that the $i-$th component of the true spectrum will be reconstructed as the $j-$th component of the measured spectrum. The naive inversion of $\mathbb{A}$ does not work because $\mathbb{A}$ is often singular. The process of solving (3.1) and thereby obtaining $\vec{b}^{true}$ is called *unfolding*. Several different algorithms may be used for unfolding. The approaches based on *Singular Value Decomposition* (SVD) [24] and Bayes' theorem [25] are presented.

Let us redefine $\vec{x} := \vec{b}^{true}$ and $\vec{b} := \vec{b}^{rec}$ for convenience.

3.2 Singular Value Decomposition

Theorem 2 (SVD). *Let $\mathbb{A} \in \mathbb{R}^{m,n}$ be an arbitrary matrix where $n, m \in \mathbb{N}$. Then $\mathbb{A}$ admits a decomposition of the form*

$$\mathbb{A} = \mathbb{U}\mathbb{S}\mathbb{V}^T, \tag{3.2}$$

where $\mathbb{U} \in \mathbb{R}^{m,m}$ and $\mathbb{V} \in \mathbb{R}^{n,n}$ are orthogonal matrices and $\mathbb{S} = \mathrm{diag}(\mathbb{S}_{11}, \mathbb{S}_{22}, ..., \mathbb{S}_{rr})$. The numbers $\mathbb{S}_{11} \geq \mathbb{S}_{22} \geq \mathbb{S}_{rr} \geq 0$ are called the singular values of $\mathbb{A}$ where $r = \mathrm{rank}(\mathbb{A})$.

The dimension of $\vec{b}^{true}$ has to be less than or equal to the dimension of $\vec{b}^{rec}$ in order to make the problem well-posed.

Suppose that $\mathbb{A} = \mathbb{U}\mathbb{S}\mathbb{V}^T$. Substituting in (3.1) for $\mathbb{A}$ gives

$$\mathbb{U}\mathbb{S}\mathbb{V}^T\vec{x} = \vec{b}, \tag{3.3}$$

$$\vec{x} = \mathbb{V}\mathbb{S}^{-1}\mathbb{U}^T\vec{b}, \tag{3.4}$$

which is easily calculated since $\mathbb{S}^{-1}$ is obtained by replacing the diagonal elements of $\mathbb{S}$ by their respective reciprocal values (provided that $\mathbb{S}^{-1}$ exists). Note that the matrices $\mathbb{U}$ and $\mathbb{V}^T$ might be viewed as rotation operators and $\mathbb{S}$ as a scaling operator for intuitive understanding of the decomposition.

In the derivation of the equations used in SVD unfolding, the main ideas of [24] are adopted. The problem with SVD arises when the singular values of $\mathbb{A}$ are zero or close to zero. In that case $\mathbb{S}^{-1}$ does not exist. Let us restate (3.1) as follows

$$\mathbb{A}\vec{x} = \vec{b} \Leftrightarrow (\mathbb{A}\vec{x} - \vec{b})(\mathbb{A}\vec{x} - \vec{b})^T = 0. \tag{3.5}$$

The problem of finding a convenient substitute for $\mathbb{A}^{-1}$ is therefore equivalent to minimising the corresponding quadratic form.

The components of $\vec{b}$ may have different statistical uncertainties in general. This is accounted for by introducing the inverse covariance matrix $\mathbb{M}^{-1}$ of $\vec{b}$ into the quadratic form.

The problem is thus equivalent to minimising the quadratic form

$$(\mathbb{A}\vec{x} - \vec{b})\mathbb{M}^{-1}(\mathbb{A}\vec{x} - \vec{b})^T = 0. \tag{3.6}$$

Furthermore, several steps will be carried out which will help eliminate the singular values of $\mathbb{A} \in \mathbb{R}^{n,m}$. First, the matrix $\mathbb{A}$ and the vector $\vec{x}$ are normalized using a presumed shape of the solution—the so-called *prior* spectrum.

Consider $\forall i \in \{1, 2, .., m\}, \forall j \in \{1, 2, .., n\}$

$$y_i = x_i / x_i^{ini}, \tag{3.7}$$

$$\bar{\mathbb{A}}_{ij} := \mathbb{A}_{ij} x_j^{ini}, \tag{3.8}$$

where $\vec{x}^{ini}$ is an initial estimate of the solution. It is obvious that $\bar{\mathbb{A}}\vec{y} = \vec{b} \Leftrightarrow \mathbb{A}\vec{x} = \vec{b}$.

The matrix $\bar{\mathbb{A}}$ respects the shape of the expected spectrum and its elements are not probabilities but counts.

The aforementioned transformation is justified for this particular use for several reasons. Using $\bar{\mathbb{A}}$ better represents errors and weights suppressing less populated bins. Another reason is that if $\vec{x}^{ini}$ is reasonably close to $\vec{x}$ then $\vec{y}$ shall be smooth and nearly constant (varying slowly).

The covariance matrix $\mathbb{M}$ from (3.6) is symmetric and positive-definite. Using Theorem 2 one gets

$$\mathbb{M} = \mathbb{Q}\mathbb{R}\mathbb{Q}^T \Leftrightarrow \mathbb{M}^{-1} = \mathbb{Q}\mathbb{R}^{-1}\mathbb{Q}^{-1}, \tag{3.9}$$

Where $\mathbb{Q}, \mathbb{Q}^T$ are orthogonal and $\mathbb{R}$ is a diagonal matrix. Substituting (3.9) in (3.6) and redefining $\hat{\mathbb{A}} = \mathbb{R}^{-\frac{1}{2}}\mathbb{Q}^T\mathbb{A}$ and $\hat{\vec{b}} = \mathbb{R}^{-\frac{1}{2}}\mathbb{Q}^T\vec{b}$ yields

$$(\hat{\mathbb{A}}\vec{y} - \hat{\vec{b}})(\hat{\mathbb{A}}\vec{y} - \hat{\vec{b}})^T = 0. \tag{3.10}$$

Thus far the quadratic form (3.10) is equivalent to (3.1) which still might be ill defined. The next step is the regularization of the problem. A regularization works around the problem of inverting singular matrices.

To regularise the quadratic form an *a priori* condition on the solution is added

$$(\bar{\mathbb{A}}\vec{y} - \vec{\bar{b}})(\bar{\mathbb{A}}\vec{y} - \vec{\bar{b}})^T + \tau\,(\mathbb{C}\vec{y})^T\,\mathbb{C}\vec{y} = 0. \tag{3.11}$$

The parameter τ represents the weight of the regularization. While this parameter is strongly problem-dependent and must be determined numerically, the *a priori* condition $(\mathbb{C}\vec{y})^T\,\mathbb{C}\vec{y}$ may be determined from general considerations.

Under the assumption that the prior spectrum has been chosen close enough to the true spectrum, it can be expected that $\vec{y}$ is a slowly varying spectrum. Since the statistical fluctuations induce oscillations in the measured spectrum therefore also in the solution, the next step will be to define and minimalize a measure which represents the curvature of the solution. The degree of oscillations can be conveniently quantified by means of second derivatives. Finite-difference methods may be used to approximate second derivatives as

$$f''(x) \approx \frac{f(x+h) - 2f(x) + f(x-h)}{h^2}. \tag{3.12}$$

Consider the sum of the squares of second derivatives of $\vec{y}$ with steps $h = 1$ to be the measure of "curvature"

$$(\mathbb{C}\vec{y})^T\,\mathbb{C}\vec{y} = \sum_i \left(y_{i+1} - 2y_i + y_{i-1}\right)^2. \tag{3.13}$$

The matrix $\mathbb{C}$ from (3.13) can be expressed as

$$\mathbb{C} = \begin{pmatrix} -1+\varepsilon & 1 & 0 & 0 & \cdots & 0 \\ 1 & -2+\varepsilon & 1 & 0 & \cdots & 0 \\ 0 & 1 & -2+\varepsilon & 1 & \cdots & 0 \\ \vdots & \vdots & \vdots & \vdots & \ddots & \vdots \\ 0 & 0 & 0 & 0 & \cdots & -1+\varepsilon \end{pmatrix}, \tag{3.14}$$

The small increment ε is added to the diagonal in order to make $\mathbb{C}$ invertible. A sensible choice for ε is on the order of $\varepsilon = 10^{-3}$ [24].

The problem thus leads to an over-determined system of equations

$$\begin{pmatrix} \bar{\mathbb{A}} \\ \sqrt{\tau}\mathbb{C} \end{pmatrix} \vec{y} = \begin{pmatrix} \vec{\bar{b}} \\ \vec{0} \end{pmatrix}, \tag{3.15}$$

of which the solution is searched by the so-called *damped least squares* method. Equation (3.15) is rearranged by factoring out $\mathbb{C}$

$$\begin{pmatrix} \bar{\mathbb{A}}\mathbb{C}^{-1} \\ \sqrt{\tau}\mathbb{I} \end{pmatrix} \mathbb{C}\vec{y} = \begin{pmatrix} \vec{\bar{b}} \\ \vec{0} \end{pmatrix}. \tag{3.16}$$

By applying SVD on

$$\bar{\mathbb{A}}\mathbb{C}^{-1} = \mathbb{U}\mathbb{S}\mathbb{V}^T, \tag{3.17}$$

one can rewrite the regularized solution of (3.16) as

$$\vec{y}^{\,\tau} = \mathbb{C}^{-1}\mathbb{V}\vec{z}^{\,\tau}, \tag{3.18}$$

where

$$z_i^\tau := \frac{d_i \mathbb{S}_{ii}}{\mathbb{S}_{ii}^2 + \tau}, \tag{3.19}$$

and

$$\vec{d} := \mathbb{U}^T \vec{b}. \tag{3.20}$$

The role of τ as a regularisation term is now obvious. When $\mathbb{S}_{ii} \to 0$, z_i^τ stays finite. The unfolded distribution $\vec{x}$ is to be obtained by rescaling $\vec{y}^\tau$ by $\vec{x}^{ini.}$.

3.2.1 Determining the regularization parameter

According to [24], the cut-off parameter τ can be determined by plotting $\log|d_i|$ versus i as in Figure 3.1. The cut-off parameter is then selected to be

$$\tau = \mathbb{S}_{kk}^2 \tag{3.21}$$

where k is the component indicated by the arrow and $\mathbb{S}_{kk}$ is the $k-$th diagonal element of the matrix $\mathbb{S}$ from SVD. The components of d_i where statistical fluctuations dominate are random

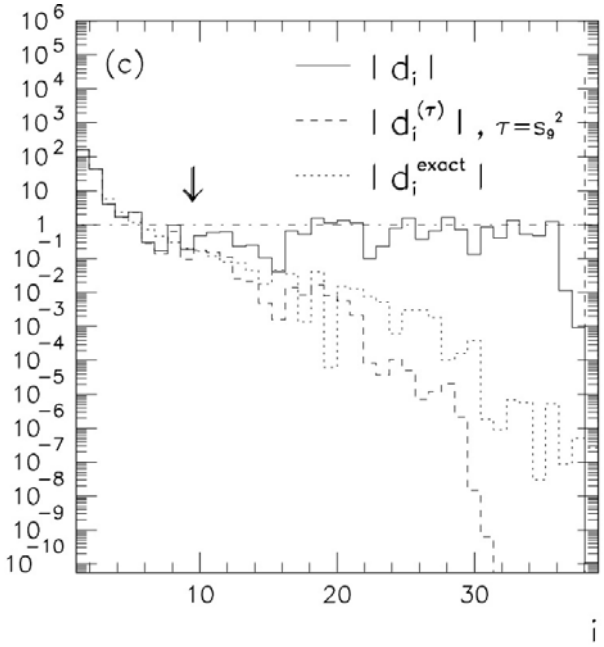

Figure 3.1: Illustration of $\log|d_i|$ versus i for choosing the optimal value for τ. Taken from [24].

numbers following $|N(0,1)|$, where $N(0,1)$ is the normal distribution with mean 0 and standard deviation 1. If $|d_i|$ vs. i is plotted,these components fluctuate around the expectation value $E[|N(0,1)|] = \sqrt{\frac{2}{\pi}}$.

3.3 A Bayesian approach

A different approach to unfolding the measured distribution is based on Bayes' theorem. Let us first state Bayes' theorem [25] upon which the unfolding is based.

Theorem 3 (Bayes). *Let C_i, $i \in [1, n_C]$ be independent causes that produce an effect E. Let further $P(\bullet|\bullet)$ be conditional probabilities. The conditional probability of C_i given E is then given by*

$$P(C_i|E) = \frac{P(E|C_i)P(C_i)}{\sum_{j=1}^{n}[P(E|C_j)P(C_j)]}, \tag{3.22}$$

where $P(C_i)$ is the probability of C_i.

Theorem 3 can be generalized to multiple effects E_j where $j \in [1, n_E]$, for each of which the conditional probability $P(C_i|E_j)$ can be found according to Theorem 3. The conditional probability $P(E_j|C_i)$ must be normalised $\left(\sum_{k=1}^{n_C} P(E_j|C_k) = 1\right)$ which implies that all effects have a cause. While no effects may happen without causes the reverse does not hold true. There might be redundant causes included. Therefore it is convenient to define a measure of efficiency $0 \leq \epsilon_i = \sum_{k=1}^{n_E} P(E_k|C_i) \leq 1$. Given N measurements of an effect E_j, the expected number of effects being caused by a cause C_i is by definition

$$N_{C_i} = N\, P(C_i|E_j). \tag{3.23}$$

Bayes' theorem has the power to *increase* the knowledge about the initial probabilities $P(C_i)$ iteratively. One can even begin without any *a priori* knowledge of $P(C_i)$ and use a uniform distribution. On the other hand, the conditional probabilities $P(E_j|C_i)$ are not effected by iterations and thus must be calculated beforehand, usually by means of Monte Carlo simulations.

The Bayesian theorem is adapted for spectra unfolding in the following way. One can associate the effect E_j with the $j-$th bin of the measured spectrum. Similarly the cause C_i corresponds to the $i-$th bin of the true spectrum which is represented by the probabilities $P(C_i)$.

Consider again the system of equations (3.1): $\mathbb{A}\vec{x} = \vec{b}$, where $\vec{x} \in \mathbb{R}^n$ is the true spectrum and $\vec{b} \in \mathbb{R}^m$ is the reconstructed spectrum. Let us identify

$$P(E_j|C_i) = A_{ij}, \tag{3.24a}$$

$$N_j = b_j, \tag{3.24b}$$

where N_j is the number of measurements of the effect E_j.

The unfolded spectrum is then given by

$$x_i = \begin{cases} \frac{1}{\epsilon_i} \sum_{j=1}^{n_E} N_j\, P(C_i|E_j), & \epsilon_i \neq 0 \\ 0, & \epsilon_i = 0. \end{cases} \tag{3.25}$$

The probability of the causes is then given by

$$P(C_i) = \frac{x_i}{\sum_{j=1}^{n_C} x_j}. \tag{3.26}$$

3.3.1 Algorithm

The algorithm for the iterative Bayesian approach to spectra unfolding might be formulated as follows

1. Chose an initial $P(C_i)^{(0)}$. In case of complete ignorance pick a uniform distribution. Further, calculate the initial $x_i^{(0)} = P(C_i)^{(0)} N_{ev.obs.}$.
2. Compute x_i according to (3.25) (using $P(C_i)^{(0)}$).
3. Determine $P(C_i)$ according to (3.26).
4. Do a χ^2 comparison between x_i and $x_i^{(0)}$, if the χ^2 is too high replace $x_i^{(0)}$ by x_i and $P(C_i)^{(0)}$ by $P(C_i)$ and go to step 2.
5. Repeat until χ^2 is sufficiently small.

Chapter 4

Simulations

The results of the previous chapter shall be now verified by toy Monte Carlo simulations. The goal is to use a reconstructed p_T spectrum of anti-k_t, charged jets and obtain the corresponding true jet p_T spectrum. Using PYTHIA 8 (v. 8.215) tune 5 [26], [27], pp collisions at $\sqrt{s} = 7$ TeV have been simulated. PYTHIA is a framework, based on C++, used for generating high-energy, elementary particle collisions. It embodies various theoretical as well as phenomenological models. In the used toy Monte Carlo method, the generated particles are distorted by detector effects—efficiency and momentum smearing. The jet clusterization routines of FastJet (v. 3.0.3) [28], [29] have been run on the PYTHIA output. The package RooUnfold [30] for the ROOT framework [31] has been used for unfolding. The RooUnfold package implements both SVD [24] and Bayesian [25] unfolding. The SVD approach is standard in data analyses and it has been used for the unfolding in the analysis.

4.1 The response matrix

Cuts applied on the particles used in this analysis are listed in Table 4.1. The cuts on η and p_T are standard in the analyses done in the ALICE collaboration [32].

Quantity	Cut value
p_T	> 0.15 GeV/c
η	$\in [-0.9, 0.9]$
state	Final state particles only
charge	Charged particles only

Table 4.1: Cuts applied to PYTHIA particles during event generation.

In the toy Monte Carlo simulation, the set of particles is duplicated. One set will remain unchanged (true particles) while the other is distorted (reconstructed particles) in order to simulate detector effects (reconstruction efficiency and momentum smearing). Particles "reconstructed" by the detector are called *tracks*.

An effect of the track reconstruction efficiency on a generated particle is simulated by a random removal of particles according to the measured track reconstruction efficiency vs. track p_T of the ALICE detector [33], see Figure 4.1. The selection algorithm is performed as follows. A random number with uniform probability distribution from the interval $[0, 1]$ is generated for

each track. If the number is greater than the appropriate efficiency shown in Figure 4.1, the track is discarded.

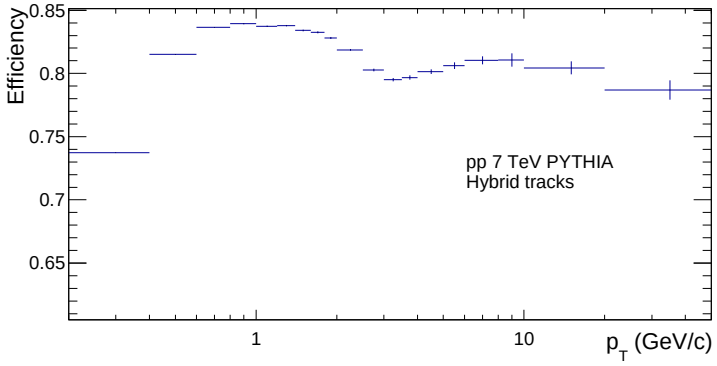

Figure 4.1: The efficiency of track reconstruction in the ALICE detector as a function of p_T. The track reconstruction efficiency corresponds to the so called hybrid tracks [33].

Furthermore, the transverse momenta of tracks are randomly distorted. The parametrization of the momentum smearing follows the paper [34]. For each track that survived the efficiency cut a random real number is generated according to the Gaussian distribution $N(0, \sigma)$ with mean 0 and standard deviation

$$\sigma = \sqrt{(0.01\, p_T)^2 + \left(0.007\, p_T^2\right)^2}. \tag{4.1}$$

The track p_T is then

$$p_{T,\mathrm{rec}} = p_{T,\mathrm{gen}} + N(0, \sigma), \tag{4.2}$$

where $p_{T,\mathrm{rec}}$ is the reconstructed transverse momentum, $p_{T,\mathrm{gen}}$ is the generated (true) transverse momentum.

After the distortions, both sets of tracks are clustered by FastJet using the anti-k_t algorithm with $R = 0.4$ using the boost-invariant p_T recombination scheme, the minimum jet constituent p_T of 150 MeV/c and restricting the jet pseudorapidity $|\eta_{\mathrm{jet}}| < 0.5$.

The sets of generated and reconstructed tracks are not identical because of the aforementioned detector effects (recall that a certain number of particles is left out and the transverse momenta are smeared). Therefore, the correspondence between generated and reconstructed jets is determined by minimizing a metric proportional to the angular distance of the two jets

$$\rho(\phi, \eta) = \sqrt{(\phi_{\mathrm{jet,gen}} - \phi_{\mathrm{jet,rec}})^2 + (\eta_{\mathrm{jet,gen}} - \eta_{\mathrm{jet,rec}})^2}, \tag{4.3}$$

where $\phi_{\mathrm{jet,gen}}$ is the azimuthal angle of the true jet, $\phi_{\mathrm{jet,rec}}$ is the azimuthal angle of the reconstructed jet, $\eta_{\mathrm{jet,gen}}$ is the pseudorapidity of the true jet and $\eta_{\mathrm{jet,rec}}$ is the pseudorapidity of the reconstructed jet.

First, for each true jet the closest (least ρ) reconstructed jet is sought. Then for each reconstructed jet the closest true jet is sought. The two jets are matched if and only if they are both the closest from the other's perspective. This eliminates the possibility that a true jet will be paired with a reconstructed jet that is closer to another true jet and vice versa.

The paired jets' transverse momenta are subsequently filled in a 2D-histogram. According to the conventions of RooUnfold, the X axis corresponds to the reconstructed jet p_T and the Y axis corresponds to the true jet p_T. A p_T spectrum of true jets is also filled to a 1D-histogram

regardless if the true jet has been reconstructed or not. The procedure of the response matrix generation is illustrated by Figure 4.2. The generated response matrix with the corresponding

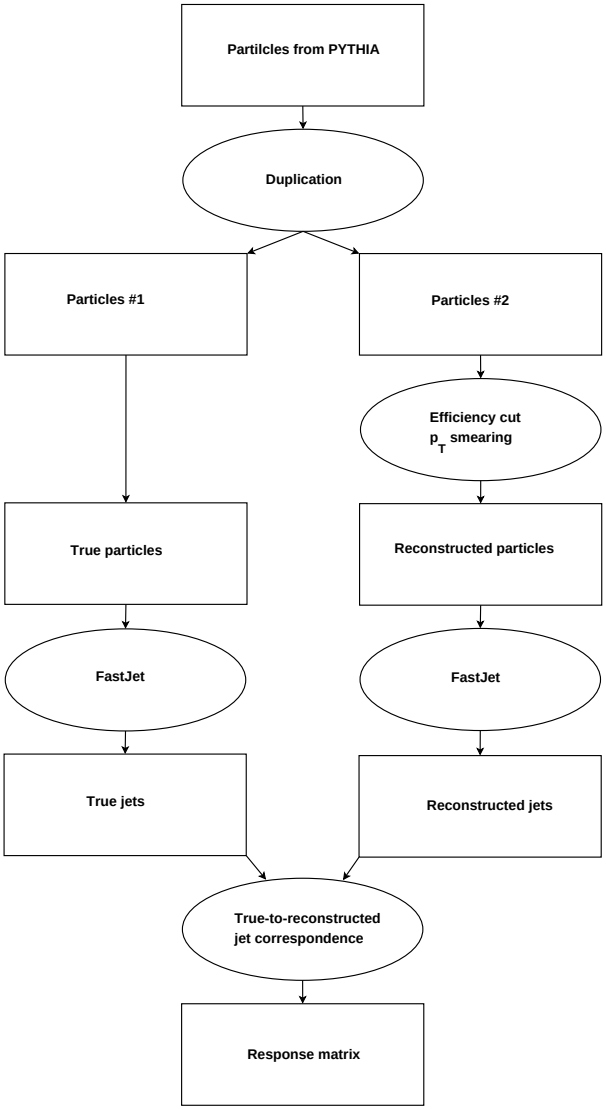

Figure 4.2: The scheme of the response matrix generation.

true jet p_T spectrum can be seen in Figure 4.3. The aforementioned true jet p_T spectrum is used in the conversion of the response matrix from cross-section to probabilities (as seen in Figure 4.4). This is done by dividing each row of the response matrix by the corresponding true p_T spectrum bin as

$$\mathbb{A}_{ij}^{\text{prob}} = \frac{\mathbb{A}_{ij}^{\text{count}}}{b_j}, \tag{4.4}$$

where $\mathbb{A}_{ij}^{\text{prob}}$ is the ij-th element of the response matrix in probabilities, $\mathbb{A}^{\text{count}}$ is the ij-th element of the response matrix in cross-section and b_j is the j-th element of the true spectrum.

The efficiency cuts are responsible for the migration of events over the diagonal of the response matrix. This is due to the fact that there are less reconstructed jets than true jets. A migration

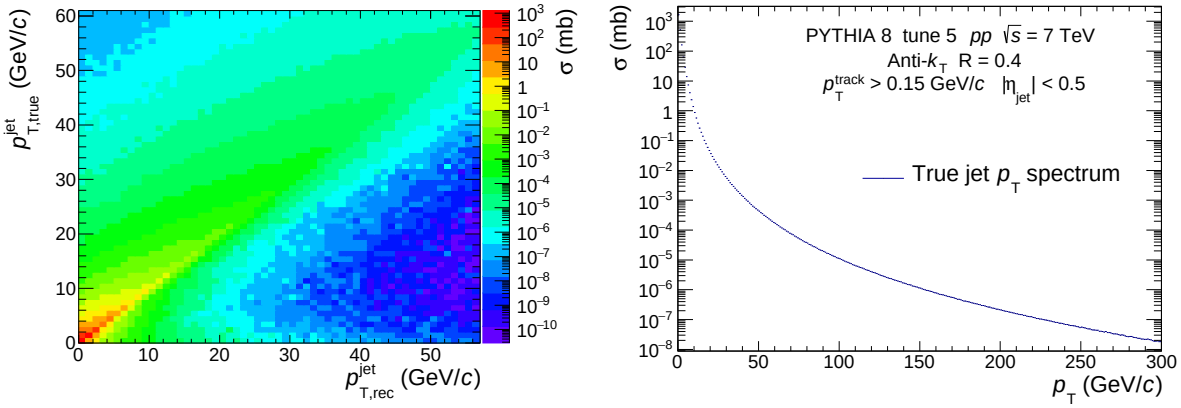

Figure 4.3: (**Left:**) The response matrix of charged, anti-k_T, $R = 0.4$ jets in pp collisions at $\sqrt{s} = 7$ TeV as generated by PYTHIA 8 tune 5. (**Right:**) The corresponding inclusive true spectrum of the charged, anti-k_T, $R = 0.4$ jets in pp collisions at $\sqrt{s} = 7$ TeV as generated by PYTHIA 8 tune 5.

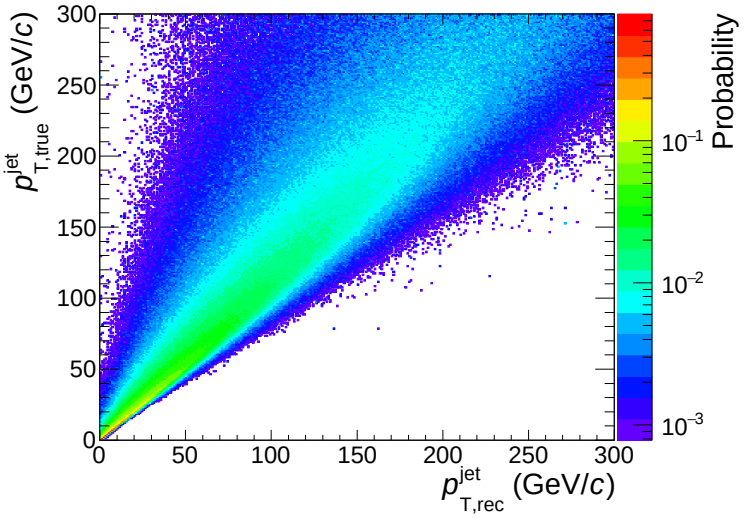

Figure 4.4: The generated response matrix of charged, anti-k_T, $R = 0.4$ jets in pp collisions at $\sqrt{s} = 7$ TeV as generated by PYTHIA 8 tune 5. The response matrix is shown in probabilities and has been generated in p_T hard bins according to 4.5.

in the opposite direction is caused by p_T smearing. The migration of events under the diagonal happens to a lesser extent for the values of p_T^{jet} are smeared in both directions.

Since the generation of a significant amount of minimum bias data to fill the response matrix would be extensively time-consuming, a different approach has been used. PYTHIA offers the option to generate collisions with constrained momentum transfer (the parameter p_T hard) which allows to gain statistics in the otherwise sparsely populated, high-p_T regions of the response matrix. This has been exploited to significantly reduce computational time.

The simulation has been split into ten consecutive intervals in p_T hard. Each interval has a fixed maximum and minimum momentum transfer. Equation 4.5 shows the border values of p_T hard bins.

$$p_T \text{ hard} = \{5, 11, 21, 36, 56, 84, 117, 156, 200, 249, 1000\} \text{ in GeV}/c \tag{4.5}$$

The resulting data is then added to form the response matrix. Selecting collisions with certain restrictions on p_T hard introduces an obvious bias. The bias is removed by weighting the partial response matrices for each momentum-transfer interval with an appropriate coefficient. The weighting coefficient is determined by the cross-section of the given p_T hard bin and the number of trials for each p_T hard interval according to the following equation

$$\left.\frac{d\sigma_{\text{jet}}}{dp_T^{\text{jet}}}\right|_{\text{MB}} = \sum_{p_T \text{ hard bin}} \frac{\sigma}{N_{\text{trials}}} \left.\frac{dN_{\text{jet}}}{dp_T^{\text{jet}}}\right|_{\text{p}_\text{T} \text{ hard bin}}, \tag{4.6}$$

where MB labels the minimum bias jet p_T spectrum, σ is the cross-section of the collisions in each p_T hard bin and N_{trials} is the number of events per the same p_T hard bin. Both σ and N_{trials} are calculated directly by PYTHIA.

4.2 Unfolding of an inclusive jet spectrum

The inclusive spectrum of charged, $R = 0.4$ anti-k_t jets in pp collisions at $\sqrt{s} = 7$ TeV is generated by PYTHIA in minimum bias mode. The same cuts have been applied as in the generation of the response matrix. The generated (true) and reconstructed (raw) spectra can be seen in Figure 4.5.

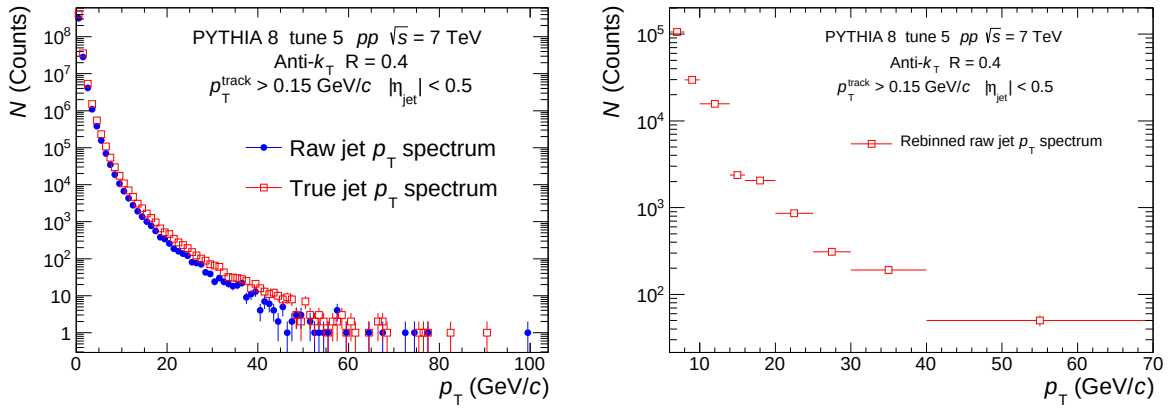

Figure 4.5: The inclusive p_T spectra of charged, anti-k_T, $R = 0.4$ jets in pp collisions at $\sqrt{s} = 7$ TeV as generated by PYTHIA 8 tune 5. (**Left:**) Comparison of the true and reconstructed spectra. (**Right:**) The raw spectrum rebinned according to (4.7) used as the input to unfolding.

Both the true and reconstructed spectra are rebinned in order to achieve at least ten counts per bin ensuring the stability of the unfolding. The set (4.7) defines the rebinning.

$$M_{\text{True}} = \{0, 4, 8, 12, 16, 20, 25, 70, 200\} \text{ in GeV}/c, \tag{4.7a}$$
$$M_{\text{Rec}} = \{6, 8, 10, 14, 16, 20, 25, 30, 40, 70\} \text{ in GeV}/c. \tag{4.7b}$$

The response matrix seen in Figure 4.4 is used. It has also been rebinned according to (4.7). The reconstructed spectrum after rebinning is shown in Figure 4.5.

A correct choice of the prior spectrum is crucial. One has to use a smooth spectrum to avoid fluctuations. The oscillations of the prior spectrum would propagate through the unfolding process and cause deviations of the unfolded spectrum from the true spectrum. The true jet p_T spectrum shown in Figure 4.5 has been used as the prior spectrum.

The spectrum is unfolded using the SVD unfolding method. SVD unfolding has been done for several values of the regularization parameter k. The optimal cut-off parameter is subsequently chosen from the resulting spectra following the procedure described in section 3.2.1. The $|d_i|$ distribution based on which the regularization parameter is assessed is shown in Figure 4.6. The

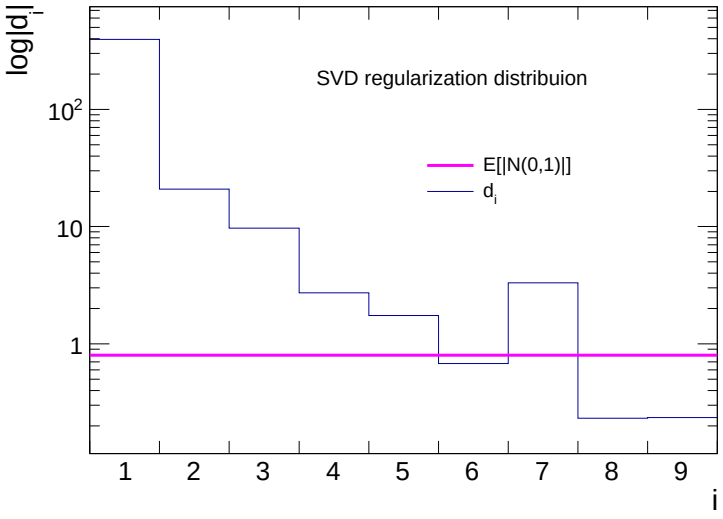

Figure 4.6: The distribution of the $\vec{d}$ vector components based on which the SVD regularization parameter is chosen. The spectrum was obtained by the unfolding of inclusive spectra shown in Figure 4.8. The purple line indicates the expectation value $E\left[\,|N(0,1)|\,\right] = \sqrt{\frac{2}{\pi}}$, where $N(0,1)$ is a normal distribution with the mean and width parameters equal to $\mu = 0$ and $\sigma = 1$ respectively. See the text for further details.

cut-off parameter has been chosen according to Figure 4.6. According to the chapter 3.2, the five rightmost values of the d_i distribution in Figure 4.6 oscillate around the purple line which shows the mean of $|N(0,1)|$. The best value of k has been chosen as $k = 5$.

To check the consistency of the unfolded spectrum, it is "folded" with the response matrix and compared to the reconstructed spectrum. The folding is done analogously to Equation 3.1. Figure 4.7 shows the comparison of the folded and raw spectra together with their ratios for several SVD regularization parameters.

Figure 4.8 shows the unfolded jet p_T spectrum compared to the true jet p_T spectrum as well as the ratios of the true and unfolded spectra for various choices of the regularization parameter.

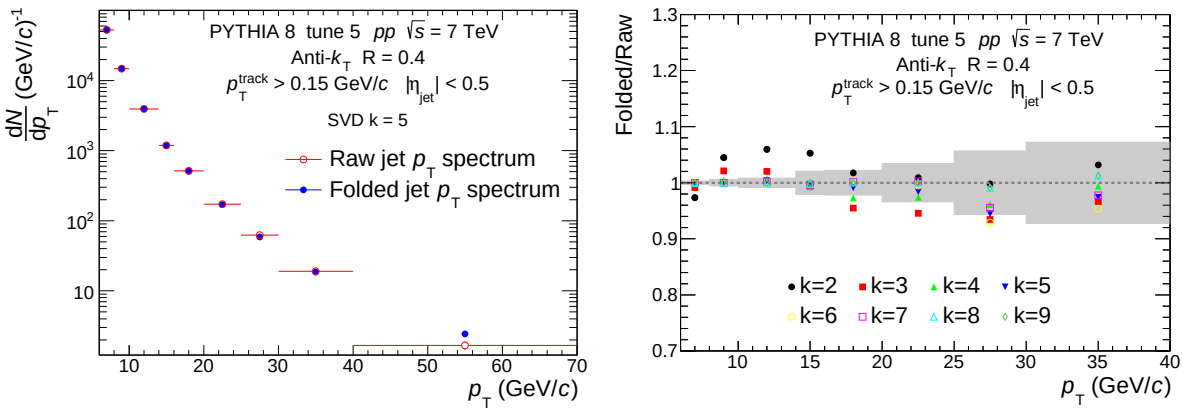

Figure 4.7: The inclusive p_T spectra of charged, anti-k_T, $R = 0.4$ jets in pp collisions at $\sqrt{s} = 7$ TeV as generated by PYTHIA 8 tune 5. (**Left:**) The folded inclusive jet p_T spectrum compared to the raw jet p_T spectrum. SVD unfolding with the regularization parameter $k = 5$ has been used. (**Right:**) The ratios of folded to raw spectra for various regularization parameters. The grey band represents the relative statistical errors of the raw spectrum.

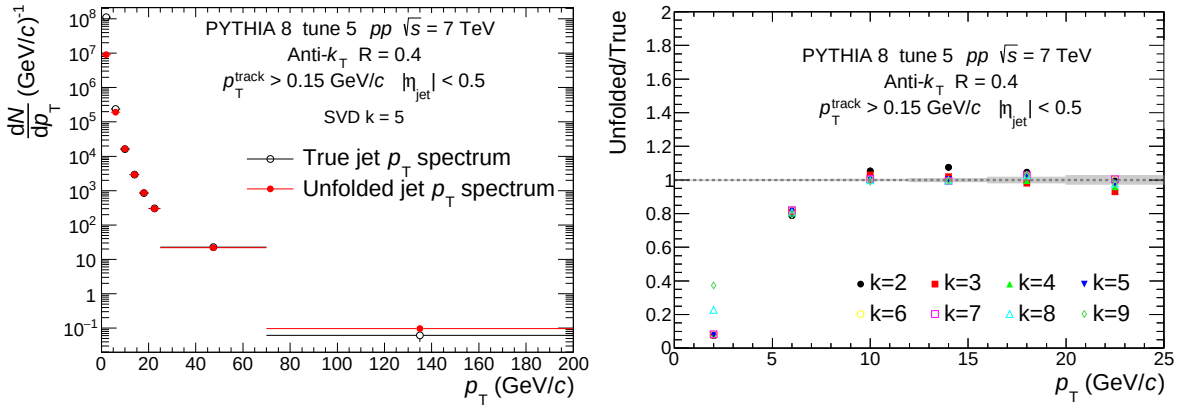

Figure 4.8: The inclusive p_T spectra of charged, anti-k_T, $R = 0.4$ jets in pp collisions at $\sqrt{s} = 7$ TeV as generated by PYTHIA 8 tune 5. (**Left:**) The unfolded inclusive jet p_T spectrum compared to the true jet p_T spectrum. SVD unfolding with the regularization parameter $k = 5$ has been used. (**Right:**) The ratios of unfolded to true spectra for various regularization parameters. The grey band represents the relative statistical errors of the true spectrum.

A good match between the true and unfolded spectra has been found for jets with $p_T \gtrsim 10$ GeV/c as seen in Figure 4.8. The observed differences between the true and unfolded spectra can be attributed to statistical fluctuations in the input true spectrum which are not caught by the unfolding. In general, the regularization should suppress fluctuations and smoothen the unfolded solution.

4.3 Unfolding of a semi-inclusive jet spectrum

In the paper [10], authors suggest using semi-inclusive spectra of hard jets to study jet quenching induced by the hot and dense nuclear matter. In order to quantify the degree of

modification induced by the medium it is also necessary to study the semi-inclusive jet production in light systems such as pp and p-Pb.

The semi-inclusive spectra of jets that recoiled from a hard p_T trigger hadron are harder than the inclusive spectra (Q^2 of the underlying hard-scattering process is much larger than for the inclusive processes) [10].

The trigger particle is searched in each event following the selection criteria listed in Table 4.1, in addition it has to have p_T constrained to $6 < |p_T^{\text{trigger}}| < 50$ GeV/c. If several particles satisfy the criteria, a random one is selected from them (semi-inclusivity). Particles with p_T higher than 50 GeV/c do not affect the selection process. The analysis is performed as follows:

1. A particle that satisfies the trigger criteria is searched in the event.
2. If an event has a trigger, jets are reconstructed.
3. Only jets that are back-to-back in azimuth, $|\phi_{\text{jet}} - \phi_{\text{trigger}}| \leq \pi - 0.6$ rad, with respect to the trigger particle are selected for the analysis.

The procedure is similar to that carried out in [10]. The resulting recoil jet p_T spectra are normalized to the number of triggers.

A modification of the previously shown unfolding process of inclusive spectra shall be outlined in order to unfold semi-inclusive spectra. The response matrix (Figure 4.4) is multiplied by the true semi-inclusive jet p_T spectrum and rebinned according to

$$M_{\text{True}} = \{0, 4, 8, 12, 16, 20, 25, 70, 200\} \text{ in GeV}/c, \tag{4.8a}$$

$$M_{\text{Rec}} = \{4, 6, 8, 10, 12, 14, 16, 20, 25, 30, 70\} \text{ in GeV}/c. \tag{4.8b}$$

The resulting response matrix is used in the unfolding of semi-inclusive spectra and is shown in Figure 4.9.

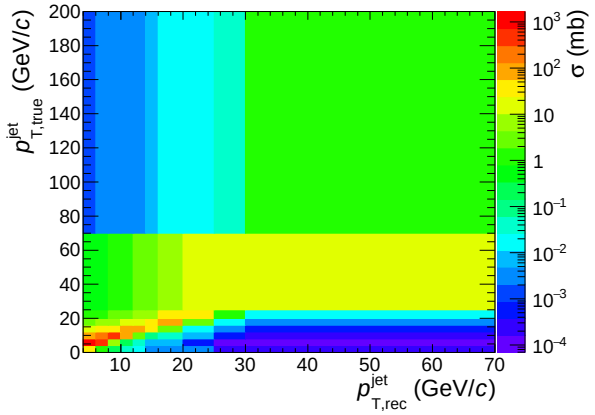

Figure 4.9: The generated response matrix for semi-inclusive spectra of charged, anti-k_T, $R = 0.4$ jets in pp collisions at $\sqrt{s} = 7$ TeV as generated by PYTHIA 8 tune 5. The response matrix is shown in cross-section after rebinning according to (4.8).

The rest of the procedure has been carried out similarly as in the inclusive case with one exception—the spectra shown are normalized to the number of triggers. The semi-inclusive spectra of charged, $R = 0.4$, anti-k_t jets have been generated by PYTHIA in minimum bias mode. The comparison of the true and raw semi-inclusive spectra is shown in Figure 4.10.

The SVD regularization distribution is visualized in Figure 4.11. The optimal regularization parameter has been chosen as $k = 8$. The comparison of the true and unfolded spectra as well as their ratio for various regularization parameters presented in Figure 4.12. The folded and raw spectra are compared in Figure 4.13.

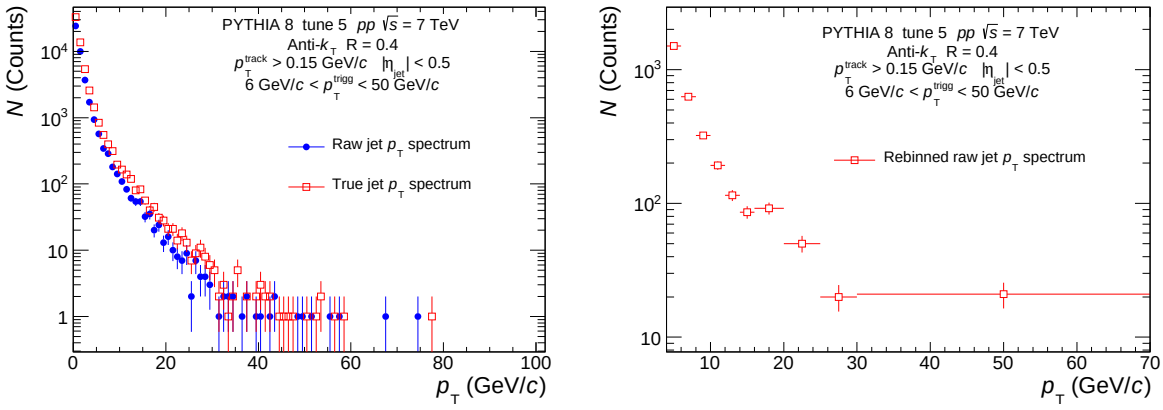

Figure 4.10: The semi-inclusive p_T spectra of charged, anti-k_T, $R = 0.4$ jets in pp collisions at $\sqrt{s} = 7$ TeV as generated by PYTHIA 8 tune 5. The cut on the p_T of the recoiled hadron is $6\ \mathrm{GeV}/c \leq p_T^{\mathrm{trigg}} \leq 50\ \mathrm{GeV}/c$. (**Left:**) Comparison of the true and reconstructed semi-inclusive spectra. The true jet spectra and the corresponding reconstructed spectra are marked by open and closed symbols, respectively. (**Right:**) The raw spectrum rebinned according to (4.8).

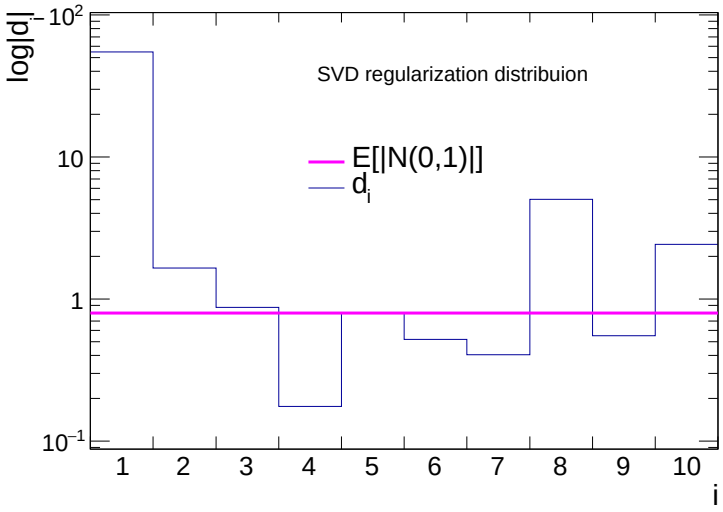

Figure 4.11: The regularization distribution for the SVD unfolding of semi-inclusive spectra shown in Figure 4.12. The purple line indicates the expectation value $E\left[\,|N(0,1)|\,\right] = \sqrt{\frac{2}{\pi}}$, where $N(0,1)$ is a normal distribution with the mean and width parameters equal to $\mu = 0$ and $\sigma = 1$ respectively.

In the current state of the analysis, Figure 4.12 (Right) suggest a slight overestimation in the unfolded spectrum. The presented results are not final and correspond to the state of the analysis. The observed 10 % discrepancy shall be subject to further examination. The discrepancy might be caused by an unsatisfactory smoothness of the chosen prior spectrum.

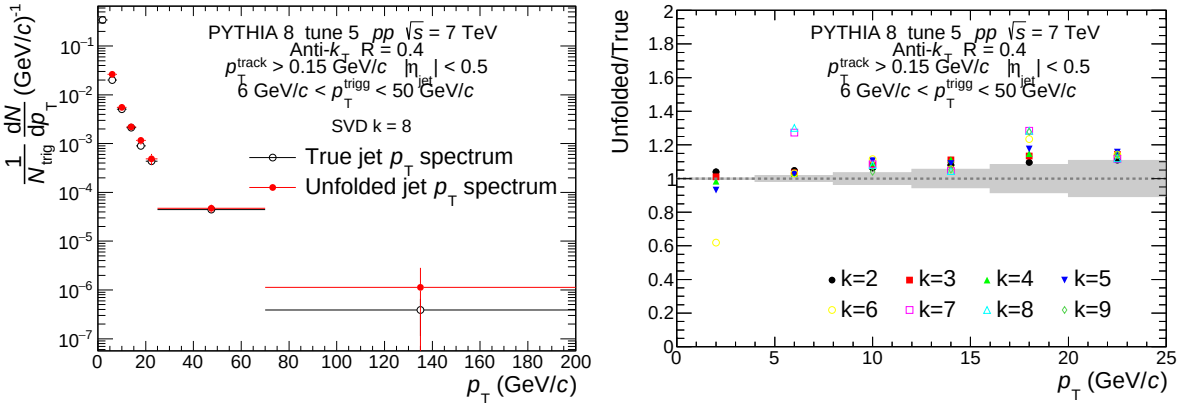

Figure 4.12: The semi-inclusive p_T spectra of charged, anti-k_T, $R = 0.4$ jets in pp collisions at $\sqrt{s} = 7$ TeV as generated by PYTHIA 8 tune 5. The cut on the p_T of the trigger hadron is $6 \text{ GeV}/c \leq p_T^{\text{trigg}} \leq 50 \text{ GeV}/c$. (**Left:**) The unfolded semi-inclusive jet p_T spectrum compared to the true jet p_T spectrum. SVD unfolding with the regularization parameter $k = 8$ has been used. (**Right:**) The ratios of unfolded to true spectra for various regularization parameters. The grey band represents the relative statistical errors for the true spectrum.

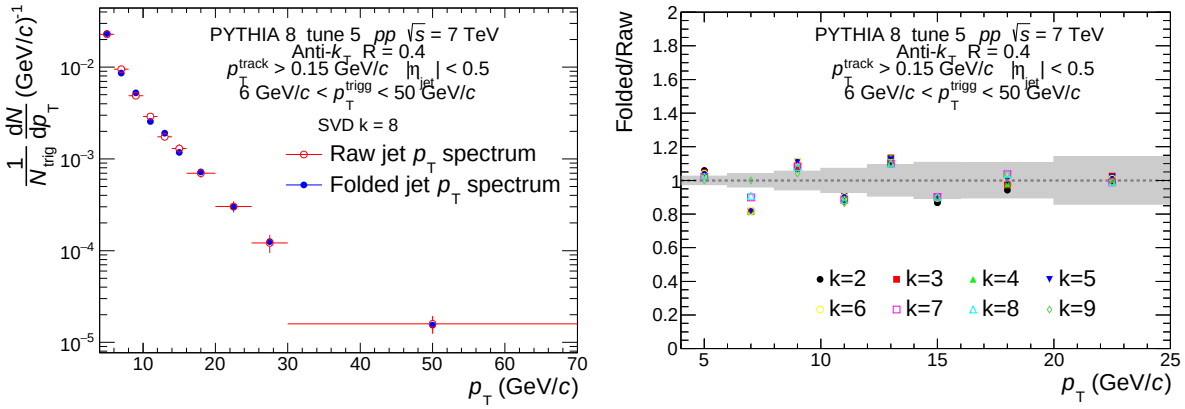

Figure 4.13: Semi-inclusive p_T spectra of charged, anti-k_T, $R = 0.4$ jets in pp collisions at $\sqrt{s} = 7$ TeV as generated by PYTHIA 8 tune 5. The cut on the p_T of the trigger hadron is $6 \text{ GeV}/c \leq p_T^{\text{trigg}} \leq 50 \text{ GeV}/c$. The grey band represents the relative statistical errors for the true (left) and raw (right) spectra. (**Left:**) The folded semi-inclusive jet p_T spectrum compared to the raw jet p_T spectrum. SVD unfolding with the regularization parameter $k = 8$ has been used. (**Right:**) The ratios of folded to raw spectra for various regularization parameters. The grey band represents the relative statistical errors for the raw spectrum.

Conclusion

Today, the microscopic description of the Strong force is based on QCD. QCD is based on the idea that interactions between quarks in hadrons are facilitated by a non-Abelian gauge theory built upon the condition of local gauge invariance of the quark fields with respect to the $SU(3)$ group.

Although quarks and gluons have never been observed as free particles, their existence is confirmed by a number of indirect observations. One of them is the existence of jets. Jets are often intuitively understood as an approximation of the quark/gluon after a hard scattering. More rigorously, jets are phenomenological objects defined by an algorithm. A very important condition on the jet algorithm is IRC safety. Only IRC safe algorithms yield theoretically consistent, finite cross-sections values. The most widely used jet algorithm is the anti-k_t algorithm which is used in a very wide range of studies from the properties of the top quark to the study of QGP.

Measured spectra of jets are inevitably distorted by physical detectors (particle reconstruction efficiency, p_T smearing). Before a comparison of the measured jet spectra to the theoretical predictions can be carried out, a correction is needed. Unfolding methods have been devised for this purpose. We present two of them, SVD and Bayesian unfolding. The key difference between Bayesian and SVD unfolding is that the Bayesian approach iteratively generates a solution based on Bayes' theorem whereas SVD uses a regularization and a numerical matrix inversion. The SVD unfolding procedure is verified using a toy Monte Carlo simulation in PYTHIA. Two cases have been studied. Inclusive jets and semi-inclusive jets. In the latter case the jet production is accompanied by a production of a high p_T particle that is back-to-back with the jet in the azimuth. Inclusive spectra have been successfully unfolded with a satisfactory precision. Semi-inclusive spectra exhibit a slight discrepancy. The presented results reflect the current state of the analysis. To find the cause of this discrepancy, the unfolding process will be repeated with a different choice of the prior spectrum and a different rebinning scheme of the response matrix and the spectra involved.

Bibliography

[1] Edward V Shuryak. Quantum chromodynamics and the theory of superdense matter. *Physics Reports*, 61(2):71–158, 1980.

[2] J. C. Collins and M. J. Perry. Superdense matter: Neutrons or asymptotically free quarks? *Phys. Rev. Lett.*, 34:1353–1356, May 1975.

[3] Tanmoy Bhattacharya et al. QCD Phase Transition with Chiral Quarks and Physical Quark Masses. *Phys. Rev. Lett.*, 113(8):082001, 2014.

[4] J. Adams et al. Transverse momentum and collision energy dependence of high p(T) hadron suppression in Au+Au collisions at ultrarelativistic energies. *Phys. Rev. Lett.*, 91:172302, 2003.

[5] C. Adler et al. Centrality dependence of high p_T hadron suppression in Au+Au collisions at $\sqrt{s}_{NN}$ = 130-GeV. *Phys. Rev. Lett.*, 89:202301, 2002.

[6] J. Adams et al. Evidence from d + Au measurements for final state suppression of high p(T) hadrons in Au+Au collisions at RHIC. *Phys. Rev. Lett.*, 91:072304, 2003.

[7] K. Adcox et al. Suppression of hadrons with large transverse momentum in central Au+Au collisions at $\sqrt{s_{NN}}$ = 130-GeV. *Phys. Rev. Lett.*, 88:022301, 2002.

[8] K. Adcox et al. Centrality dependence of the high p(T) charged hadron suppression in Au+Au collisions at s(NN)**(1/2) = 130-GeV. *Phys. Lett.*, B561:82–92, 2003.

[9] J. D. Bjorken. Energy Loss of Energetic Partons in Quark - Gluon Plasma: Possible Extinction of High p(t) Jets in Hadron - Hadron Collisions. 1982.

[10] Jaroslav Adam et al. Measurement of jet quenching with semi-inclusive hadron-jet distributions in central Pb-Pb collisions at $\sqrt{s_{\mathrm{NN}}} = 2.76$ TeV. *JHEP*, 09:170, 2015.

[11] Jiří Chýla. *Quarks, partons and Quantum Chromodynamics.* Accessed: 14.02.2016.

[12] Günther Dissertori, Ian Knowles, and Michael Schmelling. *Quantum chromodynamics.* Oxford University Press, 2005.

[13] Murray Gell-Mann. *Nobel Prize in Physics 1969 - Presentation Speech.* Noobel Media AB 2014. Accessed: 23.06.2016.

[14] Ivan Štoll and Jiří Tolar. *Teoretická fyzika.* České vysoké učení technické v Praze, 2008.

[15] Jiří Blank, Pavel Exner, and Miloslav Havlíček. *Lineární operátory v kvantové fyzice.* Karolinum, 1993.

[16] Don Colladay, Patrick McDonald, and David Mullins. Quaternionic Formulation of the Dirac Equation. In *Proceedings, 5th Meeting on CPT and Lorentz Symmetry (CPT 10)*, pages 199–203, 2010.

[17] Ta-Pei Cheng and Ling-Fong Li. *Gauge theory of elementary particle physics.* Oxford University Press, 1988.

[18] Walter Rudin. *Principles of mathematical analysis.* McGraw-Hill Book Co., New York, third edition, 1976. International Series in Pure and Applied Mathematics.

[19] Bethke and Siegfried. Experimental tests of asymptotic freedom. *Prog. Part. Nucl. Phys.*, 58:351–386, 2007.

[20] Siegfried Bethke. α_s 2002. *Nucl. Phys. Proc. Suppl.*, 121:74–81, 2003. [,74(2002)].

[21] A. R. Baden. Jets and kinematics in hadronic collisions. *Int. J. Mod. Phys.*, A13:1817–1845, 1998.

[22] ATLAS Collaboration. ATLAS events shown at the LHC seminar on physics results from run2, 15.12.2015. General Photo, Dec 2015.

[23] Gavin P. Salam. Towards Jetography. *Eur. Phys. J.*, C67:637–686, 2010.

[24] Andreas Hocker and Vakhtang Kartvelishvili. SVD approach to data unfolding. *Nucl. Instrum. Meth.*, A372:469–481, 1996.

[25] G. D'Agostini. A Multidimensional unfolding method based on Bayes' theorem. *Nucl. Instrum. Meth.*, A362:487–498, 1995.

[26] Torbjorn Sjostrand, Stephen Mrenna, and Peter Z. Skands. PYTHIA 6.4 Physics and Manual. *JHEP*, 05:026, 2006.

[27] Torbjörn Sjöstrand, Stefan Ask, Jesper R. Christiansen, Richard Corke, Nishita Desai, Philip Ilten, Stephen Mrenna, Stefan Prestel, Christine O. Rasmussen, and Peter Z. Skands. An Introduction to PYTHIA 8.2. *Comput. Phys. Commun.*, 191:159–177, 2015.

[28] Matteo Cacciari, Gavin P. Salam, and Gregory Soyez. FastJet User Manual. *Eur. Phys. J.*, C72:1896, 2012.

[29] Matteo Cacciari and Gavin P. Salam. Dispelling the N^3 myth for the k_t jet-finder. *Phys. Lett.*, B641:57–61, 2006.

[30] Harrison B. Prosper and Louis Lyons, editors. *Proceedings, PHYSTAT 2011 Workshop on Statistical Issues Related to Discovery Claims in Search Experiments and Unfolding, CERN,Geneva, Switzerland 17-20 January 2011*, Geneva, 2011. CERN, CERN.

[31] Rene Brun and Fons Rademakers. {ROOT} — an object oriented data analysis framework. *Nuclear Instruments and Methods in Physics Research Section A: Accelerators, Spectrometers, Detectors and Associated Equipment*, 389(1–2):81 – 86, 1997. New Computing Techniques in Physics Research V.

[32] K. Aamodt et al. The ALICE experiment at the CERN LHC. *JINST*, 3:S08002, 2008.

[33] Jaroslav Adam et al. Measurement of jet suppression in central Pb-Pb collisions at $\sqrt{s_{\mathrm{NN}}}$ = 2.76 TeV. *Phys. Lett.*, B746:1–14, 2015.

[34] K Aamodt et al. Transverse momentum spectra of charged particles in proton-proton collisions at $\sqrt{s} = 900$ GeV with ALICE at the LHC. *Phys. Lett.*, B693:53–68, 2010.